Department of the Navy
BUREAU of ORDNANCE
Contract NOrd-16200 - Task 1

FREE-BODY MODELING OF THE DYNAMICS OF A FIN-STABILIZED BALLISTICS MISSILE IN NONSPINNING VERTICAL TRAJECTORIES

Donald A. Price, Jr.

Hydronamics Laboratory
CALIFORNIA INSTITUTE OF TECHNOLOGY
Pasadena, California

Report No. E-73. 1

April 1957

Department of the Navy
Bureau of Ordnance
Contract NOrd-16200
Task I

FREE BODY MODELING OF THE DYNAMICS OF A FIN-STABILIZED BALLISTICS MISSILE FOR NONSPINNING VERTICAL TRAJECTORIES

Donald A. Price, Jr.

Hydrodynamics Laboratory
California Institute of Technology
Pasadena, California

Report No. E-73.1

April 1957

CONTENTS

ABSTRACT

Part 1 of an experimental and analytical investigation of the behavior in free flight of inertia-propelled bodies that are fin-stabilized is presented. The dynamic response in vertical trajectories starting from rest has been found for two sizes of a single configuration of the Basic Finner Research Missile with a variety of model parameters and initial conditions. A relatively simple formulation of the drag function for longitudinally accelerated motion in the laminar flow regime is found to give excellent agreement between predicted and experimental behavior. Time-position histories of test trajectories are presented in tabular form.

INTRODUCTION

The evaluation of a theory requires experimental data of a high order of precision and reliability. Particularly is this true in the theory of the behavior of free bodies in a fluid as expressed by equations of motion of a complex nature. An unabridged set of equations in six degrees of freedom leads to an analytically unsolvable expression for relatively simple formulations of hydrodynamic characteristics. Even the use of linearized coefficient functions in describing severely restricted regimes of motion often results in intractable equations.

Analytic solutions have been obtained for such restricted modes as stability on a straight course at essentially constant speed and for certain conditions of steady-state turning. Although unambiguous analytical solutions of the nonlinear differential equations do not exist, numerical solutions may be obtained with the aid of various computing facilities with a reasonable amount of effort. However, in order to solve a given formulation of the equations with such modern computing aids, one must be able to evaluate or measure the pertinent hydrodynamic characteristics. Present techniques using captive bodies allow measurement of static characteristics directly, but, although the general form is known, acceleration and damping functions may not be measured independently. This represents perhaps a greater hinderance than the analytical impasse, for with all coefficient functions

evaluated, regardless of form and complexity, a numerical solution can be obtained by exercising ingenuity and perseverance. Also, the accuracy with which characteristic functions are measured profoundly affects the solution. Indeed, the inability to predict trajectories of free bodies is generally attributed to the unreliability and inaccuracy of the measured data. This appears to be a very plausible explanation in view of the fact that measurements made on an identical model in different installations quite often yield different results in static coefficients.

Implicit in the evaluation of a theory is a critical examination of the structure of the equations describing that theory. The ultimate objective of the present investigation is to be a thorough examination of the theory governing the behavior in free flight of inertia-propelled bodies that are fin stabilized by a combination of experimental and analytical studies. The experimental work consists of measuring the dynamic response of a given configuration using free-flying models moving under water in the fully wetted regime in the Controlled Atmosphere Launching Tank. The analytical work consists of the prediction from theory of the behavior in free flight of these models and of comparisons of theoretical and experimental results. The hydrodynamic coefficients required for this analytical work have been measured in the High Speed Water Tunnel of this Laboratory. Two factors are present here which have heretofore been missing in such types of model experimental and theoretical studies; (a) the free-flying models in the launching tank yield accurate and detailed data for comparison with theoretical predictions, and (b) these free models and the models on which the hydrodynamic coefficients are measured in the water tunnel operate at approximately the same Reynolds number, thus eliminating any scale effects. In addition, the models used in the free flight and water tunnel are identical in configuration. As is so often the case in studies of this kind, the model configuration finally used to evaluate the theoretical predictions is somewhat different from that on which the coefficients were measured. Discrepancies between prediction and experiment may then be due to configuration change as well as evaluation of data or formulation of the equations of motion.

Although the scope of the investigation has been reduced, principally in the analytical studies, it is felt that the experimental data determined in this investigation is of sufficient precision and completeness to stimulate a thorough examination of the present state of knowledge of the equations of

motion of a body moving in fluid and of the pertinent hydrodynamic characteristics which enter these equations.

This investigation is sponsored by the Bureau of Ordnance, Department of the Navy, under Contract No. NOrd-16200 as a part of Section ReO3 Rigid Body Dynamics Program. The work in the Controlled Atmosphere Launching Tank is carried on as Task 1 of the subject contract.

Scope

The investigation has been broken down into four parts, depending upon the types of motion involved. This report describes Part 1 - Nonspinning, Vertical Trajectories - where the model is released just below the water surface and accelerated by gravity for straight and curved trajectories. The straight trajectories represent simple longitudinally accelerated motion. The curved trajectories represent accelerated planar motion with initial inclination angles.

Part 2 - Nonspinning, Horizontal Trajectories - includes families of trajectories launched at finite velocities on an initially horizontal path, decelerated by drag and curved under the influence of gravity. Parts 3 and 4 will investigate the effects of fin-induced spin and lift upon the dynamic response for the vertical and horizontal trajectories of Parts 1 and 2, respectively.

This report presents Part 1 of the study. The model construction, experimental techniques and data reduction procedures are described in detail. A brief description of the Controlled Atmosphere Launching Tank, trajectory recording system and trajectory analyzing system is given. Test results are presented in the form of curves and tables showing model positions and attitudes as functions of time for variation of weight, center of gravity position, moment of inertia and initial inclination. Scale effects are explored with two sizes of models. Analytical expressions for the drag function are derived and a method of analysis for planar motion is suggested.

MODEL TEST PROGRAM

Table 1 shows the list of tests made for Part 1 indicating the specific model size and configuration, the weight, c.g. location, moments of inertia and initial conditions for launching. Two sizes of models were used, a

one-inch diameter and a two-inch diameter of slightly differing configuration, complete descriptions of which are given in the following section. The tests listed for the one-inch diameter model are primarily of an experimental and exploratory nature; therefore this particular model was not made with as great precision as was the two-inch model. The slight difference in configuration was not considered important. Being of smaller size and less refined construction, the one-inch model did not allow as fine adjustment of the physical parameters of the shape as did the two-inch model. The principal purpose of using the one-inch model was to obtain as wide a variety of these physical parameters and also get as long a trajectory as possible in the depth of tank available. The range of the cameras and the depth of the water in the tank in general limited the length of trajectory possible to record to about eight feet, from just under the water surface to the bottom of the tank. For the one-inch model this provided about ten missile lengths of travel, whereas for the two-inch diameter it was something less than five missile lengths.

MODELS

General Configuration

The model shape used in the free-flying test is the Basic Finner Research Missile that has been used previously in aeroballistics work and is primarily a supersonic shape. The configuration is shown in Fig. 1 and is seen to consist of a sharp-pointed cone-cylindrical body with square wedge fins. All the dimensions are based on the cylindrical-body diameter. The trailing edges of the four symmetrical fins are in the plane of the trailing edge of the body.

This body shows the usual sharp-angled austerity of configuration that is common for supersonic type missiles. The nose has a sharp point, the wedge-shape fins have sharp leading edges, and there are no fillets at the junctions of the fins and the body. The center of buoyancy is noted on the drawing of the configuration. The center of gravity, being variable, depends on the weight distribution inside the model.

Model Construction

The one-inch diameter model used for the preliminary studies is shown on the right in Fig. 2. This model is of unit-type construction with

a separate nose cone and nose tip. The cylindrical portion of the body consists of a brass tube with the slots cut to accept the four fins which are joined at the center of the body by dovetailing and soldered in place. A flat disk is then soldered to close off the rear of the body flush with the trailing edge of the fins. The nose tip is separate for replacement in case of damage during launching. A soft iron magnetic pole piece is recessed into the aft end of the body for holding the model in the magnetic launcher. A threaded tie rod on the axial centerline of the model holds the nose cone and nose tip in place. Brass weights are mounted on this tie rod to vary the weight and trim of the missile. Figure 3a shows the disassembled view of the one-inch model with a weight mounted on the tie rod. The two knurled thumb screws hold the weight at a given position on the tie rod. Close examination of the photograph will show circumferential scratches and longitudinal scratches which locate the position of the painted crosses on the model as shown in Fig. 2. It may be noted from Fig. 3a that the fin shape is not exactly a wedge shape. Since this was a preliminary model the fins were made with a convenient thickness and wedge angle for strength and for ease of construction. The fin material is phosphor bronze to better withstand the wear and tear normally encountered with free-flying models. The actual configuration of the fin profiles is shown in Fig. 1. By nature of their construction the fins of the one-inch model are fixed in angle at zero degrees incidence.

The construction details of the two-inch model are shown in Figs. 3 and 4. Figure 4 shows a line drawing illustrating the arrangement of the fins, the cone and the nose tip, the tie rod and the weight tube. The fins are made separate for easy replacement, and also for adjustment to various incidence angles. The base of each fin is flat and the cylindrical contour of the body is faired-in using wax. The fins are held to the tail section by means of four small screws for each fin. The various components of the model are held together by a tie-rod assembly. This tie rod is actually a bolt and nut configuration. Two nuts at the nose end lock the rod and hold the various components together yet allow the rod to be rotated inside the model. The head end of the tie rod contains holes for a spanner wrench which allows the rod to be rotated externally while the O-rings seal the model against leakage. The ballast weights are mounted on a tube which rides on the tie rod. One end of the ballast tube is threaded to match the threads on the tie rods, so that when the tie rod is rotated the tube and

weights are shifted fore and aft, thereby changing the trim. The weights are slotted top and bottom and ride on rails fixed to the inside diameter of the body tube. The balance weights are cut in discreet increments of the buoyancy of the missile so that the specific gravity of the missile may be varied by known amounts. Each unit of ballast weight is made up by two halves so that the moment of inertia of the model may be varied merely by separating the two halves of the weight any given amount on the ballast tube. Small washers allow minor variations in the weight and for adjusting the initial buoyancy of the model. Figure 4 shows the minimum and maximum position of the weights for changing moment of inertia. The trim of the missile may be adjusted externally while submerged by means of this unique tie rod ballast tube arrangement. All joints except those of the tie rod are sealed with wax. The nose tip is held in place as well as sealed with wax. For those runs at neutral buoyancy a small buoyancy adjusting screw is included at the head end of the tie rod. This screw consists of an Allen head bolt with a groove cut in it for an O-ring. The O-ring seals the space between the threads and the head of the bolt in the tie rod. The buoyancy is adjusted by moving the screw in or out to change the size of the air space in the head of the tie bolt. This provides a minor adjustment of ± 0.002 lb buoyancy. For use in the magnetic chuck the buoyancy screw is replaced by a soft iron screw which fits flush into the recess at the base of the model. The various parts of the model may be seen in Fig. 3b showing the disassembled view of the model. Two other views of the model are shown in Fig. 5. In the rear view may be seen the soft iron magnet pole piece. The shape of the fin base may also be seen, and close examination will reveal the wax contour.

The physical parameters of both models are shown in Table 2. Included also is the range of variations possible in each model for weight, moment of inertia and trim. The actual dimensions of each model are included for comparison with the specified configuration.

Figures 2, 3 and 5 show the reference cross layout used with both models. The arrangement consists of three circumferential bands plus eight interrupted longitudinal lines spaced at 45-degree intervals on the circumference of the cylindrical portion of the body. These crosses on the body are sufficient to accurately determine all quantities except roll. In order to measure roll with sufficient accuracy, additional crosses were placed on the fins as shown. These consist of longitudinal lines near the

tip of each fin and a 45-degree line running from the forward tip of each fin to the rear junction of the fin with the body. This arrangement of the crosses allows complete determination of the position and attitude of the model with either single or stereographic projection in the trajectory analyzing device.

DESCRIPTION OF EQUIPMENT

The experimental work was carried on in the Controlled Atmosphere Launching Tank, which is described briefly in Appendix B. However, two recent improvements affecting the measuring accuracy of the tank and equipment are described in some detail here. The first improvement is a new camera film gate and the second is a system of reference crosses in the tank. A comparison of the new "slot-type" camera film gate with the original roller-type gate is shown in Fig. 6a. The previous roller gate consisted of two pairs of rollers, one pair acting as a back-up with sliding hold-down fingers at the edges. The roller pairs had an interference fit that imparted a reverse curvature to the film as it entered and left the field of view of the lens in the focal plane. This reverse curvature was intended to eliminate the transverse curvature inherent in the film due to the emulsion (noticeable in Fig. 6). However, since the film is unsupported between the back-up rollers and humidity could not be controlled sufficiently, the film curvature could not be eliminated and distance from this lens varied up to ± 0.005 inch. In addition, a curvature in the vertical plane is induced by the reverse curve when the film is in motion. Since the film is clamped flat between glass plates in the projector (Fig. 6b), the difference in curvature of the film introduced a significant error in alignment of the stereo images. Previously this curvature was matched in the projector by inserting shims between the film and glass plates. Frame to frame differences in film position were accounted for by adjustment of the magnification with the projector lens to match the reference crosses on the wall, which introduced an additional error. It was felt, for a study of this sort, that the film position should be held to within ± 0.0003 inch in order to provide sufficient analyzing accuracy. This would correspond to ± 0.02 inch in the lateral dimension in the analyzer.

The new film gate consists essentially of a slot through which the film slides with a window cut out facing the lens. An attempt is made to take advantage of the inherent transverse curvature of the film by allowing a

small amount of buckle in the slot gap which is larger than the thickness of the film yet remains within the depth of field at the focal plane. The back of the film rubs against a highly polished solid back-up block while only the edges of the emulsion side rub against the front plate. This arrangement holds the film almost flat statically. (Most of the buckling occurs in the region of the sprocket holes.) Running tests indicate that it performs equally as well dynamically. Most important, however, the film position appears to be consistent from frame to frame when pictures of the reference crosses are compared to those taken with a glass plate in place of the film.

The front plate of the gate swings toward the lens for threadingthe film loop. A spring leaf holds the plate in proper position yet deflects enough to allow the lap splice in the film loop to pass through the gate. The film is guided laterally by the shoulders which maintain the 0.010-inch gap. (The film is 0.006 inch thick.) Mechanically the gate works very well through the full range of film speeds, with only slight scratching of the back surface of the film. The presence of such fine scratches has shown no effect upon the analyzing accuracy.

The projector gate duplicates the arrangement of the camera gate except for the fact that the back-up plate is glass to allow the light to pass. The 0.010-inch gap, maintained here, also allows the film to buckle in the same manner that the film does in the camera gate. Figures 6b and 6c show the comparison of the original projector gate with the new slot-type projector gate.

Additional crosses have been painted on the rear wall of the tank in order to provide reference points over almost the entire field of view of each of the five underwater cameras. The former reference system consisted of a single cross directly opposite each camera on its lateral centerline, so that each camera viewed its own cross plus those of the adjacent cameras. The end cameras, however, had only two reference points within the field of view. The present arrangement of crosses provides nine reference points for each camera, as shown in Fig. 7 for Camera No. 6. The additional crosses are located two feet above and four feet below each original cross with corresponding crosses three feet to either side of the end crosses. The six-foot radius of the tank wall brings the top and bottom crosses forward by 3-3/4 inches and 15 inches, respectively, of the center

crosses. Each cross is 1/4-inch wide with 6-inch long legs for the new and 12-inch legs for the original references. This network of crosses covers about 70 percent of the field of view of each camera except in the vertical direction where the water surface limits the view, as shown by the reflections in Fig. 7. This arrangement of crosses provides a continuous frame by frame check on the position and curvature of the film in the projector as compared to the alignment in the camera.

These improvements in the optical system of the tank improved the accuracy of analysis by approximately two-fold in the vertical plane and five-fold in the horizontal plane.

Model Launchers - Vertical Trajectories

A new launching mechanism was constructed for the vertical launchings. Figure 8 shows the magnetic type launcher which was used for all the vertical trajectories. As shown in Part (a), it consists of an electromagnet housed in a brass case which is fastened to a long rod. The launcher assembly is supported on the tank by means of a 4-legged stand, can slide up or down in the collar and may be locked in any vertical position. The soft iron core of the magnet extends through the bottom cup. When the model is in position, a gap is maintained between this pole piece and the pole piece in the model by the rim of the cup, thus insuring that the model is fully immersed in the water before release. The sequence of operation is as follows: The launcher is lifted up near the top surface of the tank, the model is held in position, aligned with the pole piece and the current turned on. The launcher is slid down until the model is approximately one to two inches underneath the water surface. At the desired moment during the launching cycle the current to the magnet is interrupted and the model is released. A small flashlight bulb is flashed when the magnet current is broken, placing a distinctive streak on the trajectory recording film.

Horizontal Trajectories: The horizontal launchings make use of the existing air-operated launcher mounted on the horizontal centerline of the tank (see Appendix B). A new set of guide rails was constructed for the basic finner study for use with the 2-inch model. As seen in Fig. 9, this cradle consists of a horizontal cylindrical tube with four rails mounted internally at 90-degree intervals. The brass tube is lightened with a series of holes which also promote better flow of water around the missile during

acceleration. The individual guide rails may be adjusted radially to vary the clearance. An additional rail at the top of the tube guides the top fin in order to maintain a constant roll angle during acceleration. The lower rails are extended out beyond the tubes to such an extent that the center of gravity passes the end of the rails at about the time the pusher releases the model after the acceleration. The cradle tube is approximately three feet long with an additional one-foot rail extension. This provides a four-foot acceleration distance to bring the model up to speed of between 12 feet per second and 50 feet per second. The maximum acceleration experienced by the model during this acceleration stroke is on the order of 9g. Figure 9c shows the model just immerging from the launcher and also shows the arrangement of the rail extensions. The necessary clearance between the rails and the model allows a maximum initial angle on the order of 0.05 degrees. The initial launching velocity may be easily adjusted by varying the accumulator air pressure of the air-operated mechanism.

Analyzer Target

The description of the trajectory mapping device is given in Appendix B, and improvements to the film gates in the projectors have been discussed above. In order to analyze the six degrees of freedom with the basic finner ballistics missile, it was necessary to construct the analyzer target assembly shown in Fig. 10. The analyzer exploring screen, as originally constructed, was intended to use a half model, that is, the model was sectioned along the vertical plane of symmetry. In order to use a full three-dimensional model it was necessary to move the center of the model out from the target by approximately six inches and to include the measurement of azimuth angle in the target assembly. The half-scale, full-model target is mounted axially on a diameter of the half-moon sector which slides in the base in the axial plane of the model target. The azimuth angle is measured by means of the scale on the sector and the vernier attached to the base. Azimuth positioning is by means of a hand screw to the right end of the base. The roll is driven and recorded by the hand screw and counter arrangement at the upper end of the sector. Part (b) shows the assembly mounted on the analyzer mechanism so that the target assembly will rotate in pitch around the c.b. of the model in the plane of a half-moon sector. The three linear dimension-- longitudinal, vertical and lateral, and the inclination angle are

recorded from the console, while the roll angle and the azimuth angle are measured on the target assembly itself. The lines on the half-model target duplicate the centerlines of the crosses painted on the model, as shown in Fig. 5. With this arrangement it is possible to measure the attitude and position of the model in all six degrees of freedom with either single projector analysis or stereo projector analysis.

A different target assembly was used for analyzing the one-inch diameter runs or trajectories. This arrangement is shown in Fig. 11. It consists of a half-model, half-scale target sliced along the axial centerline and mounted on a flat card. This card is mounted on the mechanism so that the c.g. of the target is at the center of rotation of the traversing assembly. The card may be rotated ± 16 degrees in roll by means of the small hand screw seen at the left side and the roll angle measured to the nearest one-half degree by the pointer and scale at the right. It will be noted that the target of the model consisted merely of a half-cylinder representing the cylindrical portion of the model with the nose cone and the fins omitted. This target provided measurement of five degrees of freedom—the three linear dimensions, roll and inclination. Trajectories with the one-inch model were selected for a negligible change of yaw or azimuth.

TEST PROCEDURES

Model Preparation

Prior to each test run the model weight, moment of inertia, c.g. position and fin angles are determined and adjusted according to the schedule listed under "Test Program". The buoyancy and longitudinal trim of the model are measured in the flotation tank, as shown in Fig. 12. For test runs with weight other than equal to buoyancy the weight of the model is adjusted to the required multiple of the buoyancy determined in the tank. The longitudinal position of the center of gravity, center of buoyancy and the moment of inertia may be measured and adjusted using the device shown in Fig. 13. This C-GI. balance consists of a clamping ring with a transverse stub shaft supported by precision micro ball-bearings with a torsion wire clamped at a third support. The balance frame is doweled to the model measuring plate so that the ring is clamped on the model at the scaled longitudinal c.g. location on the body axis. With the model adjusted

to neutral buoyancy the longitudinal trim is adjusted in the flotation tank, as illustrated in Fig. 12, by adjusting the weights inside the model until the pointer returns to the zero position. Upon removing the model and balance from the water, the c.g. location may be determined by moving the balance weights along the rods until the rod again recenters (see Fig. 13a). This gives the displacement of the center of gravity and center of buoyancy from the centerline of the bearings. Once the center of buoyancy position is determined in this manner, the longitudinal trim may be adjusted regardless of the weight or specific gravity. With the balance rods removed and the balance set on end, the model may be oscillated about the bearings against the torsion wire and the period of oscillation compared to that of the calibrating rod to determine the moment of inertia, as shown in Fig. 13b. The use of this device allows measurement of centers of gravity and buoyancy to within one thousandth of an inch and radius of gyration to within two-thousandths of an inch.

The sequence of launching operations described in Appendix B is typical of the test runs made here. After the test run, the buoyancy, longitudinal trim and fin angles are checked and the model then prepared for the succeeding test.

RESULTS

Experimental results and applicable analysis of the data are presented in the series of curves and tables shown in Figs. 14 through 19 and in Tables 3 and 4. The curves for Phase 1a – straight vertical trajectories – are given in Figs. 14 through 17 as functions of time. Since these curves have been plotted to a large scale and subsequently reduced greatly, the corresponding tabular data is listed in Table 3. The experimental results of Phase 1b – curved vertical trajectories – are shown in Figs. 18 and 19 with the corresponding tabular data being given in Table 4. The reduction procedures in arriving at the tabular data are explained in Appendix B. A discussion of the accuracy and probable errors and their causes is given in Appendix B also, along with a table showing the estimated accuracies in the various dimensions.

In the figures presented, the experimental data are shown as discreet points. The line curves drawn through the experimental points indicate the

analysis of that particular run according to the equations developed in Appendix A. The nomenclature in presenting the data on the curves and in the tables is listed in Table B-2 of Appendix B showing the sign convention and its application to the present work.

DISCUSSION

Phase 1a - Straight Vertical Trajectories

A number of exploratory trajectories were run using the one-inch model with two modifications of the fins – configurations A and B and at an arbitrary specific gravity of 2.2. The principal purpose of these trajectories was to develop the launching technique, method of analysis, and to determine the limits of accuracy that are possible with such a small model. Figure 14 illustrates typical data as determined for the four runs under the same conditions with one change of the fin configuration. The depth history indicates that the trajectory response is quite consistent with very small dispersion. The velocity curve gives a measure of the accuracy of analysis. The data points represent the first difference of the tabular data of depth versus time with no averaging of the raw data. The velocities have been plotted to a rather large scale to illustrate the accuracy of the data and to show variations in the velocities. The effect of the different fin configurations (Run No. F-8) is slight but of a significant amount (see Fig. 1 for configurations of the fins). Runs Nos. F1 and F2, incidentally, had a string or thread trailing from the base for these two runs, the purpose of which was to halt the model short of the bottom of the tank to prevent damage to the nose. These runs were also released by hand, whereas Runs Nos. 6 and 8 were released by the magnetic launcher. The zero position was determined from the initial slope of the velocity curves, as may be seen from the experimental data of the velocity points. (The signal light was added after these tests.) The small dispersion shown for the depth is within the spread of the accuracy of the data or the estimate of the zero time. The line curves show the computed trajectories using the technique outlined in Appendix A. The constants of these equations were determined by successive approximations from comparison of computed and experimental velocity and depth histories. Only hand and desk calculator methods were used. It is seen that the agreement is good up to almost 10 ft per sec in both cases, and is well within the normal scatter of the experimental data. Transition of the boundary layer

from laminar to turbulent for this model is expected to occur at about 7-1/2 or 8 *ft per sec.*, which is about where the velocity curve deviates from the computed curve. No attempt has been made to compute the "turbulent" portion of these curves since these runs were of an exploratory nature. The computing procedure used is long and laborious, and the fit illustrated here is considered close enough for these particular trajectories.

The effect of variation of specific gravity upon the acceleration characteristics of the one-inch model with fin configuration "B" is shown in Fig. 15. Except for the very first portion of Run F-9, an excellent fit with the experimental data is illustrated for the computed trajectories. It is felt that a better fit to this Run F-9 may have been obtained with further refinement and successive approximations of the calculations, but the effort did not appear to be worth while. One purpose of Phase 1a of the test program was to attempt to obtain a measure of the virtual mass effects where this virtual mass is represented by the symbol, k_1, in the equation

$$m_o(1 + k_1)\, a_x = W - B - C_D\, \rho \frac{A}{2}\, V^2 .$$

This concept of incorporating the effect of drag due to acceleration into the mass term appears mathematically convenient for reducing the complexity of the equation – provided, of course, that a linear relationship between drag and acceleration exists. The effect of virtual mass in the above formulation is seen to be a reduction of acceleration in direct proportion to the applied force. If it were possible to measure such an effect one would expect to find it most pronounced at the initial portion of the trajectory where the acceleration is greatest. The maximum possible acceleration for each weight (that due to gravity in a vacuum) is illustrated by the dashed lines asymptotic to each velocity curve in Fig. 15. If virtual mass effects were detectable using this model, then the velocity curves would have an initial slope different from the dashed lines, as shown. The experimental data shown in Fig. 15 appears to indicate that added mass is either not significant or is masked out by the inaccuracies of the data. It is unfortunate that where large added mass effects may be expected, the experimental data is necessarily of poor order, as illustrated by Run No. F-9 with the specific gravity 1.28. On the other hand, where the data is better, the effects of virtual mass are somewhat smaller, so that again it is difficult to separate such effects. To illustrate the effect of virtual mass, a second series of dashed

lines is shown which were determined for an added mass equivalent to 10 per cent of the displacement of the body. It is seen that extremely accurate data is necessary for this regime of motion, or that a means of obtaining constant accelerations of a high magnitude are necessary in order to show the effects of virtual mass. In the analysis made here, the effect of virtual mass has been considered as an additional drag due to acceleration and, therefore, has been included in the drag function. The excellent fit of the computed trajectories and the relatively simple formulation of the drag function seem to justify this approach.

Figure 16 illustrates a series of tests similar to those shown in Figs. 14 and 15 using the 2-inch diameter model for a range of specific gravities from 1.1 to 4. The specified configuration of the fins, i.e., configuration "C", was used for these tests (see Fig. 1). The experimental data shown in Fig. 16 is of a somewhat higher order of accuracy than previously shown. This results from two reasons: (1) the 2-inch diameter model presents a much larger image which, consequently, is easier to align; (2) the new projector film gate, which better aligns the film in the projector, was used. The velocity data shown has been averaged over two successive intervals. Experimental data also illustrates the excellent consistency and small dispersion of repeat runs for the 2-inch diameter model. A more accurate measure of the zero time, i.e., the moment of release from the magnetic launcher, was obtained for these runs by the addition of the small signal light to the launching mechanism. The signal light is flashed, thus putting a streak on the film, at the instant the current is interrupted to the magnet. The very small delay time in release due to the breakdown of the magnetic field has been measured and is accounted for in aligning the curves.

The computed trajectories, as indicated by the line curves, are seen to be in excellent agreement with the experimental data. After the experience gained from computing the trajectories in Figs. 14 and 15, it was possible to arrive at such agreement in three or four successive approximations for each trajectory. The curve for specific gravity of 4.0(Runs Nos. 47 and 48), however, represents the first trial of the calculations. The value of the constant was determined from an extrapolation of the constants at the other specific gravities. The expected accelerations at each specific gravity in a vacuum and with an added mass of 10 percent displacement are also shown by the dashed lines asymptotic to the corresponding velocity curves. Here

again it is seen that the virtual mass effects are not significant or are masked out by the inaccuracies of the data in the initial portion of the trajectory. Again, where the added mass effects would be greatest, the accuracy of the data is smallest, and where the effects of added mass are the least, the accuracy of the data is the greatest.

If a better measure of the local or instantaneous acceleration were obtainable from the experimental data, it may have been possible to resolve the virtual mass question. Sample acceleration data for specific gravity of 2 is shown along with the computed acceleration to illustrate the scatter in the instantaneous acceleration. These acceleration points shown are average differences of the averaged velocity curves and yet still show sufficient scatter such that the actual acceleration may not be determined. Thus it appears that for the laminar regime of motion, at least, this technique of determining the drag and virtual mass effects is not adequate inasmuch as a higher degree of accuracy is necessary to obtain a good measure of acceleration.

It may be noted that for the velocity curves at specific gravity of 2 and 4, two computed curves are shown labeled "laminar" and "turbulent". The latter represents an attempt to compute the drag through transition and into the turbulent regime of motion by assuming a constant drag coefficient. It appears that the transition is of very short duration and it does not appear to affect a subsequent trajectory to a great extent. Thus it appears that an average constant drag coefficient in the turbulent regime may be assumed and applied with a fair measure of accuracy.

Formulation of Drag Coefficient

The constants of the drag function used for the computed trajectories illustrated in Figs. 14 through 16 are plotted against Reynolds number in Fig. 17a and compared with the coefficient of friction drag for a flat plate in laminar and turbulent flow. All coefficients have been referred to the cross-sectional area of the model. The effect of specific gravity on the drag coefficient is clearly shown by the displacement of the line for each model diameter, and the effect of the size of the model is shown by the displacement of the coefficient functions at each diameter for a given specific gravity. This latter fact, the "scale" effect, is merely due, however, to the choice of the Reynolds number as a parameter, as illustrated in Fig. 17b. Here the constants of the drag coefficient are found to vary with the

accelerating force, a_o, the Reynolds number and the ratio of the diameters of the model. The data points were determined by the best approximation of the computed curve to the experimental data as shown in Figs. 14 through 16. A least squares fit of these points yielded the linear relationship for K as a function of a_o. The constant drag coefficients used for computing the motion through transition and into turbulent regime of motion is also illustrated in Part (a). Since insufficient trajectory length was available in the turbulent zone, no attempt has been made to correlate these constant drag coefficients as a function of a_o.

Since the use of the laminar flat-plate, skin-friction line yields such close agreement with the trajectory data, the turbulent skin-friction line immediately suggests itself for use in passing through the transition range and into the turbulent regime until a constant drag coefficient is obtained that is equivalent to the static drag coefficient measured in the water tunnels. This does not appear to be worthwhile computing due to the short length of trajectory that is possible in the launching tank when the model is running in the turbulent regime.

Static Drag Coefficients

Figure 18 illustrates an attempt to evaluate the static drag at terminal velocities for a specific gravity 1.1 using the 2-inch model. Because of the short length of trajectory available in the tank (5-6 lengths), the model was released above the water surface in an attempt to accelerate it to approximately the terminal velocity. The curves shown indicate that in the first case the velocity was greater than the terminal velocity and in the second case was lower, so that an asymptotic approach from both sides of the terminal velocity was obtained. However, another factor enters in which makes the results somewhat questionable. Due to the blunt base shape of this model a cavity is drawn in with the model which existed for almost half of the trajectory length. Just how much effect this had upon the acceleration or deceleration of the model is not known; however, by extrapolation the terminal velocity of 4.25 fps is indicated by the curves. This corresponds to a static drag coefficient of 0.493, which is within 2.5 per cent of the value determined in the High Speed Water Tunnel of this Laboratory.

Phase 1 b - Curved Vertical Trajectories

The purpose of Phase 1 b was to determine the response of the Basic Finner to variations of specific gravity, center of gravity position, moment of inertia and initial inclination angle at release for curved vertical trajectories starting from rest. The experimental results are shown in Figs. 19 through 21 and Table 4. A preliminary calculation indicated that the general response of the model to the various initial conditions and model parameters is amenable to a relatively simple formulation of hydrodynamic functions and equations of motion.

Figures 19a and 19b show the response of the model for curved trajectories at a specific gravity of 1.1 for variations of center of gravity position. The response is as would be expected for the variations shown in the title block. By comparison with the trajectory for c.g. and c.b. coincident, we find slower turning with movement of the c.g. aft. This results in a greater longitude displacement and a relatively smaller depth displacement with time. Conversely, when the c.g. position is moved forward of the c.g., we see a much faster response in turning. There appears to be some oscillation in inclination which is larger than the normal scatter of analysis (± 0.1 degree); however, no relation between the test parameters and the wavelength of the oscillation has been found. These curves also indicate the effect of the initial conditions in inclination. It will be seen from the first portion of the curves that the inclination was not always exactly the same. This is due to the method of mounting the launcher in the Controlled Atmosphere Launching Tank. It was necessary to extend the magnet on a long bar which had some flexibility. In replacing the launcher after mounting the model, it could not always be put back into exactly the same place. However, the same general response in the inclination is noticed for all the curves regardless of the initial inclination angle.

The effect upon the velocities in the horizontal and vertical directions is masked out by the variation in the initial inclination angles, except for Run No. 37. Here the large static moment applied is reflected in the faster buildup of the vertical velocity and suppression of the horizontal velocity.

The relative effect of the difference in initial inclination is seen by a comparison of Runs Nos. 39 and 44 with Runs Nos. 41 and 43. The difference in inclination appears to be maintained approximately throughout the full trajectory.

The effect of increase in moment of inertia as compared with a shift in c.g. is shown in Figs. 20a and 20b. The influence is most pronounced in the inclination history in a manner to be expected. The increase in moment of inertia is seen to oppose the angular acceleration and deceleration, while aft movement of the c.g. opposes only angular acceleration. The additive effect of c.g. shift appears about equal to that for moment of inertia increase for the particular values listed in the figure. The trend noted in Fig. 19 is illustrated more clearly here since the initial inclination angles are more nearly equal. Figure 20b illustrates these effects most clearly in the depth versus longitude curve by increasing deviations of the trajectories with increase of moment of inertia and aft shift of the center of gravity. An oscillation in the inclination response is also clearly evident.

The influence of specific gravity is illustrated in Figs. 21a and 21b. A direct comparison is complicated by the inherent change of moment of inertia with specific gravity of the model and the difference in initial inclination angle. With increasing weight, the effect of increasing moment of inertia is obscured by the faster buildup of the hydrodynamic forces. However, its influence is shown in Figs. 19 and 20.

The inclination response of Run No. F-19 in comparison with F-50 and F-51 indicates relatively little effect of moment of inertia changes at greater specific gravity, and hence higher accelerations.

The investigation reported herein is unique in the restriction of the motion to the laminar and transition flow regimes under influence of variable acceleration. This is outside the usual range of "practical" problems encountered in hydroballistics. However, the experimental information presented herein is felt to be of sufficient accuracy and breadth to lead to a usable formulation of the equations of motion for these conditions.

The numerical trajectory data for the curves presented in Figs. 14 through 21 are given in Tables 3 and 4 for use in curve fitting with various techniques and formulations of the equations of motion. The time values shown in the left-hand columns are determined by the flash rate of the stroboscopic Edgerton lamps of the tank. Since the release time is arbitrary with respect to the lamp flash times, zero time is selected as the first frame recorded after the signal light flash. The corrected zero time is shown in the "t_o" line. The corrected zero positions and attitude are

also indicated at the head of each column. In those test runs where the release point and early portion of the trajectory were missing on the film record, the positions and attitude before release were clearly defined by several frames where no displacement was detected. The initial conditions are denoted by d_o, ℓ_o, and θ_o.

An extensive analytic investigation of the response of the Basic Finner model was not made for Phase 1b. However, an analysis is suggested in Appendix B which is designed for particular application to the tabular data presented in Tables 3 and 4. The trajectory histories obtained from the Controlled Atmosphere Launching Tank consist of primary measurements in horizontal, lateral and vertical positions and inclination, azimuth and roll attitudes, whereas the primary quantities in tunnel or towing tank measurements are force, angle of attack and total velocity. These directly measured quantities of the force system are second and thirt order quantities of the orthogonal trajectory system. This suggested analysis attempts to reconcile this fundamental difference between force and trajectory systems, and to select variables incorporating the highest possible degree of measuring accuracy of each system. An additional complication is introduced by requiring large angles of attack from 0^o to 90^o. It is recognized that for motion in the turbulent regime of flow the force and moment functions are no longer regular due to separation. However, in the regime of flow of interest here (laminar), the force function appears regular. Measurements at low Reynolds number on the one-inch model indicated the formulations given in Appendix B.

With the equations of motion written in this manner, one primary quantity (the angle of attack) in the force system then corresponds to the body attitude (inclination), a primary quantity in the trajectory system. Hence, the accuracy of determination of the variables approaches the highest possible degree in both systems.

SUMMARY

The dynamic response of the Basic Finner Research Missile has been determined for straight and curved vertical trajectories accelerated by gravity from rest. The trajectory histories for a wide range of model parameters and initial conditions are presented in the form of curves and tables. Experimental techniques, model design and construction, facility

improvements and data reduction procedures are described in some detail. An analysis for computing accelerated curved trajectories is suggested for particular application to the type of data obtained in the Controlled Atmosphere Launching Tank.

CONCLUSIONS

1. A formulation of the drag function was obtained for longitudinally accelerated motion in the laminar flow regime and through the transition region. For laminar flow the drag may be expressed as

$$\text{Drag} = K_D / \sqrt{R}$$

where $$K_D = 5.05 + 0.148\ a_o$$

and $$a_o = \frac{G - 1}{G} g .$$

2. The drag function through transition was found to be constant for a given value of a_o but no correlation was obtained due to lack of data. A steady-state drag coefficient was estimated from terminal velocity to be

$$C_D = 0.493 .$$

3. An attempt to evaluate an added mass term compatible with the steady-state turbulent drag coefficient was not successful.

4. Time-position data of a high order of precision has been obtained for vertical curved trajectories for use in analysis of the dynamic response of the Basic Finner Research Missile.

ACKNOWLEDGMENTS

The writer wishes to acknowledge the contribution of many members of the Hydrodynamics Laboratory to the study described herein. Especially he is indebted to Mr. V. V. Smith for his excellent work in conducting the experimental tests and to Mrs. L. Gaard for her patient and accurate analysis of the trajectory records, reduction of data and preparation of the curves. Thanks is due also to Miss Ann Rankin who typed the text and to Mrs. Jean Clough who prepared the figures.

REFERENCES

1. Levy, J. and Price, D. A., Jr. "Free Body Modeling of the Stability and Control of Submarines", California Institute of Technology, Hydrodynamics Laboratory Report No. E-27.2, May,1956 (Confidential)

2. Knapp, R. T., Levy, J., O'Neill, J. P., and Brown, F. B., "The Hydrodynamics Laboratory at the California Institute of Technology", Trans. ASME, No. 5, Vol. 70, pp. 437-457, July, 1948.

3. Knapp, R. T., "Special Cameras and Flash Lamps for High Speed Underwater Photography", Journal of Society of Motion Picture Engineers, Vol. 49, No. 1, July, 1947.

APPENDIX A

EQUATIONS OF MOTION

Phase 1 a - Longitudinal Accelerated Motion

A one-degree of freedom equation is considered

$$\frac{W}{g} a_y = W - B - \text{Drag}, \tag{1}$$

$$\text{where drag} = C_D \rho \frac{A}{2} V^2$$

$$\text{and} \quad C_D = f(a_y, V_y) .$$

In the laminar flow region, drag is due principally to friction. The variation of C_D with velocity is taken from the flat plate friction formulation

$$C_{D_V} = \frac{1.33}{\sqrt{R}}$$

and the contribution due to acceleration is assumed additive as

$$C_{D_a} = \frac{f(a_y)}{\sqrt{R}}$$

The equation (1) then becomes

$$\frac{W}{g} a_y = W - B - \frac{1.33 + f(a_y)}{\sqrt{R}} \tag{2}$$

and $f(a_y)$ is evaluated by fitting Eq. (2) to the trajectory for each value of W.

Phase 1 b - Nonspinning Planar Motion

A three-degree of freedom set of equations is considered. Forces and moments developed by the total velocity vector and angle of attack of the force system, shown in Part (a) of Fig. A-1, are broken down into components in the horizontal and vertical directions and considered due to the appropriate components of velocities of the trajectory system as shown in Part (b).

It is immediately apparent that if one considers the velocity components in the horizontal and vertical directions, the inclination angle and its

complement ($\beta = \pi/2 - \theta$) are analagous to the angle of attack of Part (a). Using the sign convention shown in Part (b) one may write directly

$$(3)\quad \begin{cases} m a_x = L_y - D_x - F_y \\ m a_y = L_x - D_y - F_x + W - B \\ I \ddot{\theta} = M_y - M_x - K_y - K_x - M_\theta \end{cases}$$

where the subscripts refer to the relevant velocity component.

Writing in coefficient form, equations (3) become:

$$(4)\quad \begin{cases} m a_x = C_{Ly} \rho \frac{A}{2} V_y^2 - C_{Dx} \rho \frac{A}{2} V_x^2 - C_{Fy} \rho \frac{Ad}{4} q V_y \\ m a_y = C_{Lx} \rho \frac{A}{2} V_x^2 - C_{Dy} \rho \frac{A}{2} V_y^2 - C_{Fx} \rho \frac{Ad}{4} q V_x \\ I_{xy} \theta = C_{My} \rho \frac{Ad}{2} V_y^2 - C_{Mx} \rho \frac{Ad}{2} V_x^2 - C_{Ky} \rho \frac{Ad^2}{4} q V_y - C_{Kx} \rho \frac{Ad^2}{4} q V_x \\ \qquad - W \bar{x}_G \cos \ddot{\theta} . \end{cases}$$

The consequence of writing the equations in this manner is the requirement that the force and moment functions be known for angles of attack far greater than normally measured with captive models. Force measurements on a one-inch diameter Basic Finner for angles of attack of $0^\circ \leq \alpha \leq 90^\circ$ indicate a simple trigonometric form of the force function. Therefore the coefficient functions were defined as follows:

For <u>turbulent</u> flow:

$$(5a)\quad \begin{cases} \text{Drag} & C_D = a_{D1} - a_{D2} \cos 2\alpha \\ \text{Lift} & C_L = a_L \sin 2\alpha \\ \text{Moment} & C_M = a_M \sin 2\alpha \\ \text{Damping moment} & C_K = a_{K1} - a_{K2} \cos 2\alpha \\ \text{Damping force} & C_F = a_{F1} - a_{F2} \cos 2\alpha \end{cases}$$

For <u>laminar</u> flow, the coefficients are assumed to follow the flat-plate friction form to give:

$$
(5b)\quad \begin{cases} C_D = \dfrac{K_D}{\sqrt{R}}\,(1 - a_D \cos 2\alpha) \\ C_L = \dfrac{K_L}{\sqrt{R}} \sin 2\alpha \\ C_M = \dfrac{K_M}{\sqrt{R}} \sin 2\alpha \\ C_K = \dfrac{K_K}{\sqrt{R}}\,(1 - a_K \cos 2\alpha) \\ C_F = \dfrac{K_F}{\sqrt{R}}\,(1 - a_F \cos 2\alpha) \end{cases}
$$

Now let:

$$
A_0 = \rho \frac{A}{2m}\sqrt{\frac{v}{\ell}} \qquad A_2 = \rho \frac{Ad}{2I_{xy}}\sqrt{\frac{v}{\ell}} \qquad A_4 = \frac{W - B}{m}
$$

$$
A_1 = \rho \frac{Ad}{2m}\sqrt{\frac{v}{\ell}} \qquad A_3 = \rho \frac{Ad^2}{2I_{xy}}\sqrt{\frac{v}{\ell}} \qquad A_5 = \frac{W_{xG}}{I_{xy}}
$$

and substituting in Eqs. (5-b) and (4), we have:

$$
(6)\quad \begin{cases} a_x = A_0 K_L V_y^{3/2} \sin 2\beta - A_0 K_D V_x^{3/2}(1 - a_D \cos 2\theta) - A_1 K_F q V_y^{1/2}(1 - a_F \cos 2\beta). \\ a_y = A_0 K_L V_x^{3/2} \sin 2\theta - A_0 K_D V_y^{3/2}(1 - a_D \cos 2\beta) + A_1 K_F q V_x^{1/2}(1 - a_F \cos 2\theta) - \\ \quad + A_4 . \\ 0 = A_2 K_M V_y^{3/2} \sin 2\beta - A_2 K_M V_x^{3/2} \sin 2\theta - A_3 K_K q V_y^{1/2}(1 - a_K \sin 2\beta) \\ \quad - A_3 K_K q V_x^{1/2}(1 - a_K \sin 2\theta) - A_5 \cos\theta . \end{cases}
$$

For the purposes of simplifying the calculations, Eq. (6) may be reduced by noting that for the coordinates shown with $0 \leq \theta \leq 90^\circ$ and $0 \leq \beta \leq 90^\circ$:

$$
\sin 2\theta = \sin 2\beta
$$

$$
\cos 2\theta = -\cos 2\beta .
$$

Then Eqs. (4) become:

$$a_x = A_0 K_L V_y^{3/2} \sin 2\theta - A_0 K_D V_x^{3/2}(1 - a_D \cos 2\theta) - A_1 K_F q V_y^{1/2}(1 + a_F \cos 2\theta)$$

$$a_y = A_0 K_L V_x^{3/2} \sin 2\theta - A_0 K_D V_y^{3/2}(1 + a_D \cos 2\theta) + A_1 K_F q V_x^{1/2}(1 - a_F \cos 2\theta) + A_4 .$$

$$0 = A_2 K_M V_y^{3/2} \sin 2\theta - A_2 K_M V_x^{3/2} \sin 2\theta - A_3 K_K q V_y^{1/2}(1 + a_K \cos 2\theta) - A_3 K_K q V_x^{1/2}(1 - a_K \cos 2\theta) - A_5 \cos\theta .$$

From which:

$$\dot{\theta} = \dot{\theta}_o + \int \ddot{\theta} dt , \quad \theta = \theta_o + \int \dot{\theta} dt$$

$$V_x = V_{x_o} + \int a_x dt , \quad x = x_o + \int V_x dt$$

$$V_y = V_{y_o} + \int a_y dt , \quad y = y_o + \int V_y dt$$

The values of A_0, A_1, A_2, A_3, A_4 and A_5 are determined by the physical parameters of the model and fluid.

The values of a_D, a_L, a_M, a_K and a_F are determined by fitting the force and moment data with the trigonometric functions (5).

The remaining constants for laminar flow (K_D, K_L, K_M, K_K and K_F) are determined by fitting equations (6) to the experimental trajectories for the corresponding physical parameters of the model.

APPENDIX B

DESCRIPTION OF THE FACILITY

The model tests are performed in the Controlled Atmosphere Launching Tank (Fig. B-1) which was originally designed and built for the study of the water entry of free-flying bodies. However, the facility is so constructed that it is well-suited for a number of other types of studies involving hydrodynamic phenomena as well. The first extension of the usefulness of the launching tank (a study of the stability and control of submarines by means of self-powered, self-controlled, free-flying models) is described in Ref. 1. This study also represented the generalization of the tank and models to six degrees of freedom. The present investigation has resulted in further refinement of the measuring accuracy and range of the facility.

Since the launching tank and its associated equipment have been described fully in Refs. 1, 2 and 3, only a brief description is included here.

The Tank

The tank consists of a large horizontal cylinder, 13 ft in diameter by 29 ft long, to one side of which is attached a section of a smaller cylinder 6 ft in diameter and 23 ft long. A battery of five 35 mm high-speed movie cameras, mounted on the horizontal centerline of this "bulge", record the underwater trajectory. Electronic flash lamps which intermittently illuminate the interior of the tank are installed in six lucite tubes which pass through the bulge above and below the cameras. Additional cameras and flash lamps are mounted in the air space to record the air flight and water entry of bodies launched with the centrifugal launcher. Auxiliary submersible flash lamps aid in spotlighting the underwater trajectories. The tank is filled to about 2-1/2 ft above the centerline (total depth 9 ft) with approximately 25,000 gallons of distilled water. This water is continuously filtered through sand and alum filters and exposed to ultraviolet lamp radiation at the surface in order to maintain maximum optical clarity. A 3/32-inch thick lining of a polyvinyl chloride plastic ("Koroseal") prevents corrosion of the tank shell and consequent contamination of the water, provides a dark background and protects models from abrasion damage. Nylon protective nets and blankets may be installed to prevent damage to the free-flying models by collision with the tank walls. The one-inch mesh net is stretched between ring bolts spotted around the tank wall by means of lines

and pulleys for easy installation and removal.

Model Launching Mechanisms

Three general types of launching mechanisms are used on the tank which allow a wide variety of initial conditions.

Centrifugal Launcher: Water entry studies make use of a centrifugal launching wheel mounted on the underside of the main hatch cover. The model is held in the "chuck" by means of a steel ribbon stretched to just below the ultimate stress. With the hatch cover lowered, the wheel is rotated at the desired speed by the electric motor drive to provide a range of tangential velocities from 50 to 180 fps. A planetary gear train maintains the model axis at a constant attitude. The model is released by shearing the ribbon at the desired rotation angle of the wheel. The model attitude may be adjusted relative to this "trajectory" angle over an angle of attack range of $\pm 10^{\circ}$ while the trajectory angle may be varied from 10° to 90° with respect to the horizontal.

Linear Launchers: Two versions of a straight line launcher mechanism are used for accelerating models up to initial speeds in as short a stroke as possible for fully submerged regimes of motion. An air-operated launcher mounted on the horizontal centerline of the tank below the centrifugal launcher consists of two major components - (1) the actuating mechanism and (2) the interchangeable guide rails. The actuating mechanism (see Fig. B-2) consists of a 3-inch I.D. cylinder and a one-piece piston and rod mounted externally with the rod extending into the tank through an O-ring seal. An air flask holds the compressed air for driving the piston, while the air cushion ahead of the piston in the cylinder stops the piston and rod at the end of its stroke. In its starting position, as shown, the piston covers the air inlet port and thus acts as a quick opening valve to start the launching stroke.

The interchangeable guide rail cradle is mounted inside the tank co-axial with the cylinder. Adjustable brass rails guide the model as it is ejected by the piston rod and also support the end of the rod and pusher during the acceleration stroke. The cradle assembly is bolted to a mounting plate hinged at the tank wall so that it may be tilted up toward the water surface for installation of the model and then lowered into position co-axial with the piston rod. The design of the interchangeable cradle is dictated by the

requirements of the particular model used in each study.

The air-operated linear launcher has an operating range of 12 to 80 fps with the normal air supply pressure of 85 psi. The mechanism is designed for a maximum of 250 fps using a 2000 psi pressure in the accumulator and a controlled cushion pressure. Initial velocities are consistent to ± 0.5 fps over the normal range of 12 to 50 fps.

A spring-operated launcher mechanism is used for velocities in the range from 1 to 10 fps. This mechanism may be fitted into the guide rail cradle and the whole assembly attached to a variable angle mount which may be positioned horizontally or vertically in the tank. The accelerating mechanism consists of a 50-pound coil spring and piston-damper unit mounted coaxial with the guide rails. A variable orifice in the damper exhaust provides control of the velocity within ± 0.1 fps over the operating range.

Trajectory Recording System

The model trajectory is recorded by a battery of high-speed motion-picture cameras using 35 mm film in conjunction with a large battery of synchronized high-intensity flash lamps. The maneuvering space and the optical coverage of the cameras is shown in Fig. B-3. Almost complete stereoscopic coverage of the maneuvering volume is available from the tank centerline to the rear, while toward the cameras only saw-tooth shaped volumes are covered. However, the model may be seen in any position by at least one camera. This multiple coverage makes it possible to use stereoscopic techniques for analysis of the recorded data to obtain six components of motion -- longitudinal, lateral and vertical movements, and rotation in the inclination, azimuth and roll.

The underwater cameras consist of a lens and film guide assembly permanently mounted on the tank with a detachable film magazine containing a 32-ft long continuous film belt. The lens is a 1-in., f/2.3 Bausch and Lomb Baltar mounted at the center of a spherical correcting window which eliminates distortion due to refraction at the water-glass interface. The lens has a field of view of 53 degrees which provides a 50 percent overlap of coverage of adjacent cameras at the centerline of the tank. The film in each camera is driven by a common drive shaft at constant speed and the exposure is made by intermittent illumination of the darkened tank interior

with the high-speed flash lamps. Each film belt is measured and spliced to exactly the same length (by counting sprocket holes) so that it may be brought up to speed gradually and yet utilize the full length for recording the trajectory. An indexing device on the camera drive allows initiation of the model run at any of twelve positions along the film loop. A series of crosses painted on the back wall of the tank provide a reference system for each frame exposed.

Tank Illumination. The model trajectory is lighted (intermittently) by high-intensity, short-duration gas-discharge flash lamps (see Ref. 3). Power for each flash lamp is provided through an individual pulse generator mounted in racks behind the tank and a 100 kva transformer primary power supply. All units are triggered by a single frequency generator and controlled in number of flashes by a timer. A frequency range of 50-3000 cps is available with a light output of about 4-watt-sec per flash.

Trajectory Analyzing System

The data analyzing or trajectory mapping system is essentially a one-half scale reproduction of the trajectory recording system of the launching tank plus an image tracking device. A general view of the analyzer room is seen in Fig. B-4, wherein the projectors replace the cameras and an exploring target assembly replaces the model. The lens of each projector is matched in focal length and depth of field to the corresponding camera lens on the tank. Because of the spherical window in the tank, the images are projected in the analyzer room geometrically correct except for a slight increase in magnification due to the deletion of the water. This difference in magnification affects only the lateral dimensions in projection. The film is advanced frame by frame simultaneously in all projectors by a hand-operated, common drive-shaft. The frame is located behind the lens by aligning the projected images of the reference crosses with corresponding reference crosses on the back wall of the analyzer room. The light source consists of an incandescent bulb and condensing lens with a water cell and forced air cooling to maintain a low film temperature. The two optical systems are very precisely aligned by measurement of the camera and reference cross positions, and checked by means of special photographic targets.

The image tracking device consists of a moving bridge and carriage

arrangement with three degrees of linear motion and two degrees of angular motion. These motions are motor driven and controlled by push buttons from the control console. The motions are followed and indicated by selsyn repeater units which drive indicating counters on the console. The third angular motion (roll) is incorporated into the model targets which are designed and built specifically for each study.

Data Reduction Procedures:

The procedures for reduction of the data on the film record to a usable form may be divided into three steps: (a) analysis of the film record (read-off), (b) computations, and (c) curve plotting.

Film Analysis. A frame-by-frame technique is used in mapping the trajectory for a given test run. The individual camera films are placed in the corresponding projectors and synchronized so that frames taken at the same time will be projected simultaneously. (A "sync" frame is placed on the stationary films before each test run by a short burst of the flash lamp.) The technique of analysis of a pair of simultaneous images is as follows: First the film is advanced by hand to the desired frame and the images of the reference cross are aligned by adjusting the film behind the lens to match those marked on the wall of the analyzer room. If necessary, the magnification is adjusted by moving the lens slightly. The target is then moved into the correct linear and angular positions by fusing the projected images of the model crosses and the target crosses. Once the two images fuse onto the target at the correct locations denoted by the centerlines of the crosses, the positions as indicated on the target assembly scales and on the counters of the console are recorded. The film is then moved onto the next frame, aligned and the procedure repeated. The trajectory history is thus mapped out frame-by-frame throughout the full length of the trajectory.

Computations: The data as received from the trajectory mapping device consists of a tabulation of the six degrees of freedom for each frame analyzed versus time. This tabular data gives the position to the center of buoyancy of the target directly for longitudinal and vertical dimensions, and for angles or attitudes in inclination and roll directly. However, for the lateral dimension and the azimuth dimension a slight correction is necessary for the shrinkage in the lateral dimension due to deletion of the spherical

window and projection in air. This correction consists of a linear expansion of the lateral distance and the tangent of the azimuth angle. The factor of expansion of these quantities is equal to the ratio of the focal plane distance in the projector to that in the camera. For the present alignment of the optical system this expansion factor is equal to 1.065.

The tabular data is first reduced by a successive differencing scheme from which rates of change for angles and displacements are obtained. A second successive differencing yields accelerations and angles of attack. A numerical integration and expansion to model size is then performed simultaneously on the differenced data. The formuli used, along with a description of the symbols, is shown in Table B-1. The difference quantities as denoted by the operator, Δ, represent the analyzed dimensions, i.e., one-half scale. The rates of change or velocities usually represent values averaged over three successive data points (1, 2, 3) in the following manner:

$$\text{Ave } \frac{\Delta\theta}{\Delta t} = \frac{1}{2}\left(\frac{\theta_2 - \theta_1}{t_2 - t_1} + \frac{\theta_3 - \theta_2}{t_3 - t_2}\right).$$

The linear or angular accelerations are expressed in a similar manner. The intervals between data points are selected on the basis of model velocity so that no appreciable error is introduced in constructing distances traveled or the rates of change from the chord segments rather than from the true arc lengths of the trajectory.

Sign Convention: The sign convention agrees with the established arrangement of the tank and analyzer system. Table B-2 shows the positive direction and defines each quantity listed in Table B-1. The convention is seen to follow the right-hand rule except for the control surface angles which are considered positive when causing a positive displacement of the primary quantities. Rates of change and angular velocity are positive for positively increasing values of the primary dimensions.

Accuracy of Data: The accuracy and consistency of the measured trajectories depends upon four factors: (1) the accuracy with which the models and targets are constructed, (2) the ability of the film gates to position the film accurately, (3) the quality of the images on the recording film, and (4) the reading ability of the analyst. The accuracy of the models, targets and the film positioning has been discussed above. An example of

the type and quality of the images obtained with the 35 mm cameras is shown in Fig. B-5. Two simultaneous images of the two-inch model are shown in this figure. The quality of these images depends upon, first, the water clarity, second, the intensity of the light sources, third, the focus of the cameras, and fourth, the effectiveness of the film emulsion. The film used for these tests is Eastman Kodak Tri-X panchromatic emulsion, which is extremely high speed and especially sensitive to the blue spectrum present in the Edgerton flash lamps. The clarity of the water is maintained by first softening and vapor pressure distillation of the water source, and then continuous filtering through sand and alum filters to maintain the clarity of the water. As may be seen by Fig. B-5, the images are of excellent quality and represent the typical quality of the images as seen throughout the tank by any given pair of cameras. The images are seen to have an excellent depth of field; the distance from the camera lens to the crosses on the back wall of the tank is approximately sixteen feet, while the distance to the model itself is approximately ten feet. The near point of the depth of field is approximately six feet from the camera, so that the full maneuvering area of the tank is within the depth of field of the cameras. As explained in Appendix B and Refs. 1 and 3, the depth of field in the tank is much greater than that in the analyzer due to the spherical correcting window and the water-filled object space. When the images are reprojected in the analyzer the depth of field is approximately 24 inches. A slight movement of the film may move this position of best focus a considerable distance, so that for certain frames the picture may be slightly out of focus with a consequent fuzziness of the image. This may be accounted for by variation of the aperture of the lens. Small changes in the position of the film,which requires a change in magnification in the analyzer, and any fuzziness of the images lead to certain errors in the projected position of the image. These, coupled with the normal human reading errors of adjusting the target to the image to get the best fit, lead to the estimate of reading accuracy shown in Table B-3. These are the figures as determined in the analyzer and are to one-half scale of those in the tank.

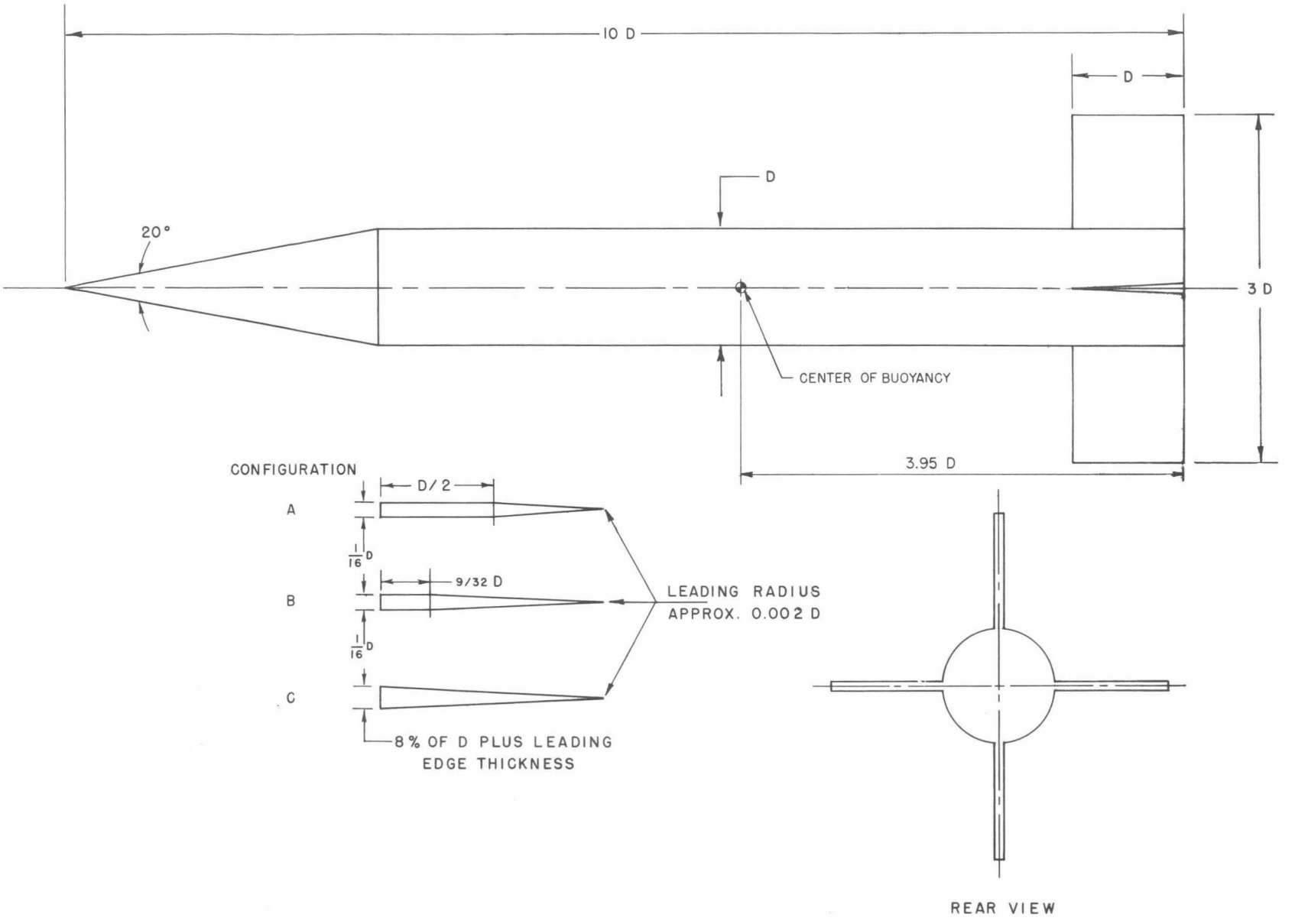

Fig. 1 - Basic Finner research missile configuration.

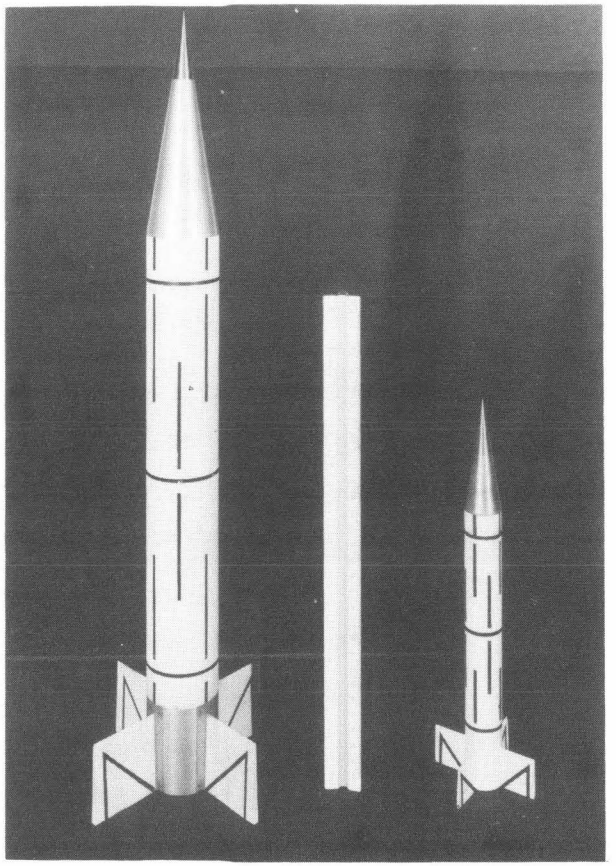

Fig. 2 - One- and two-inch diameter CALT Basic Finner launching models.

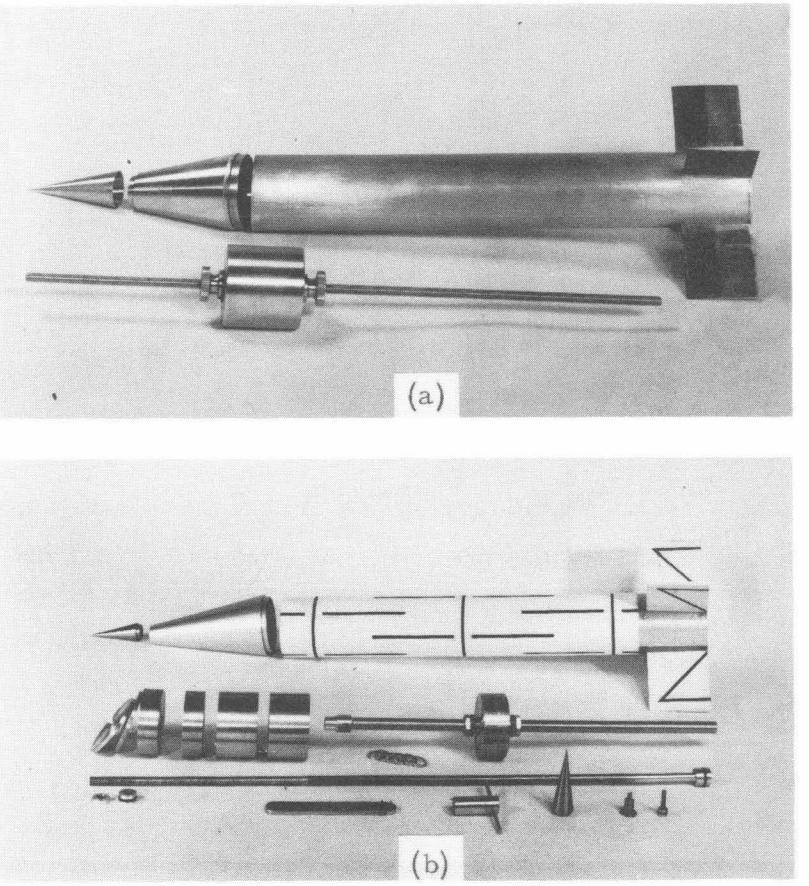

Fig. 3 - Disassembled models showing details of construction and ballast weights: (a) one-inch diameter model, (b) two-inch diameter model.

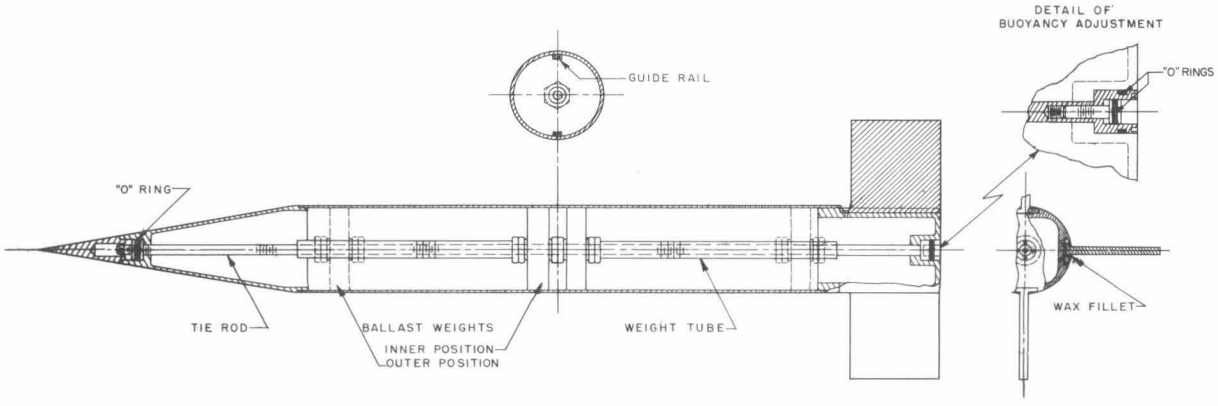

Fig. 4 - Line drawing of the two-inch diameter model showing internal construction and ballast and trim mechanism.

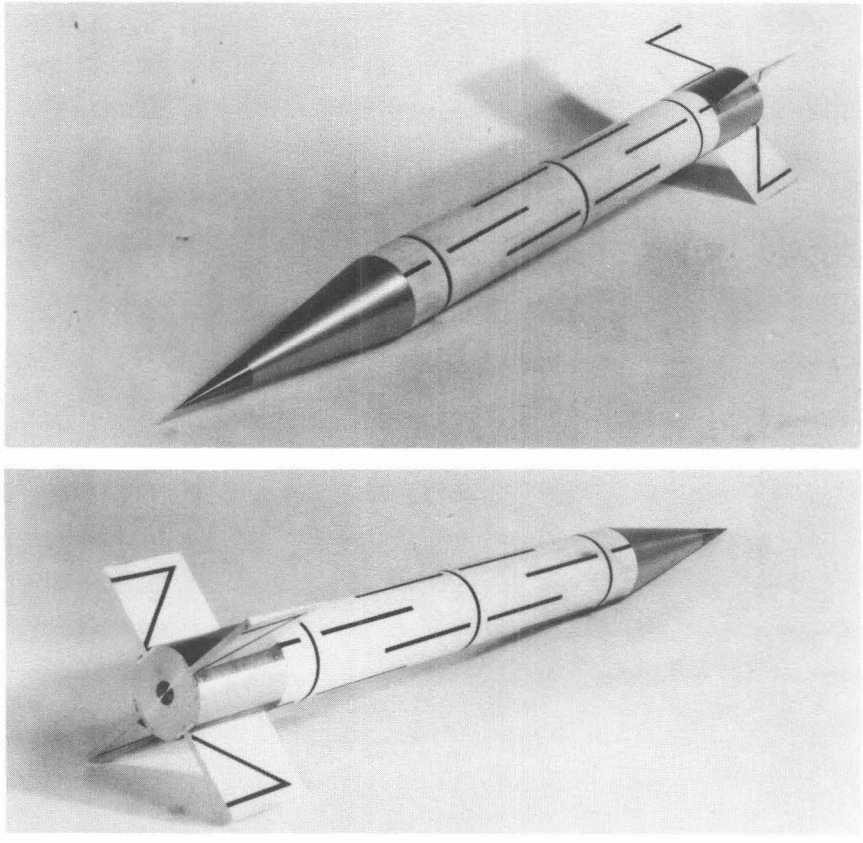

Fig. 5 - Front and rear views of the two-inch launching model.

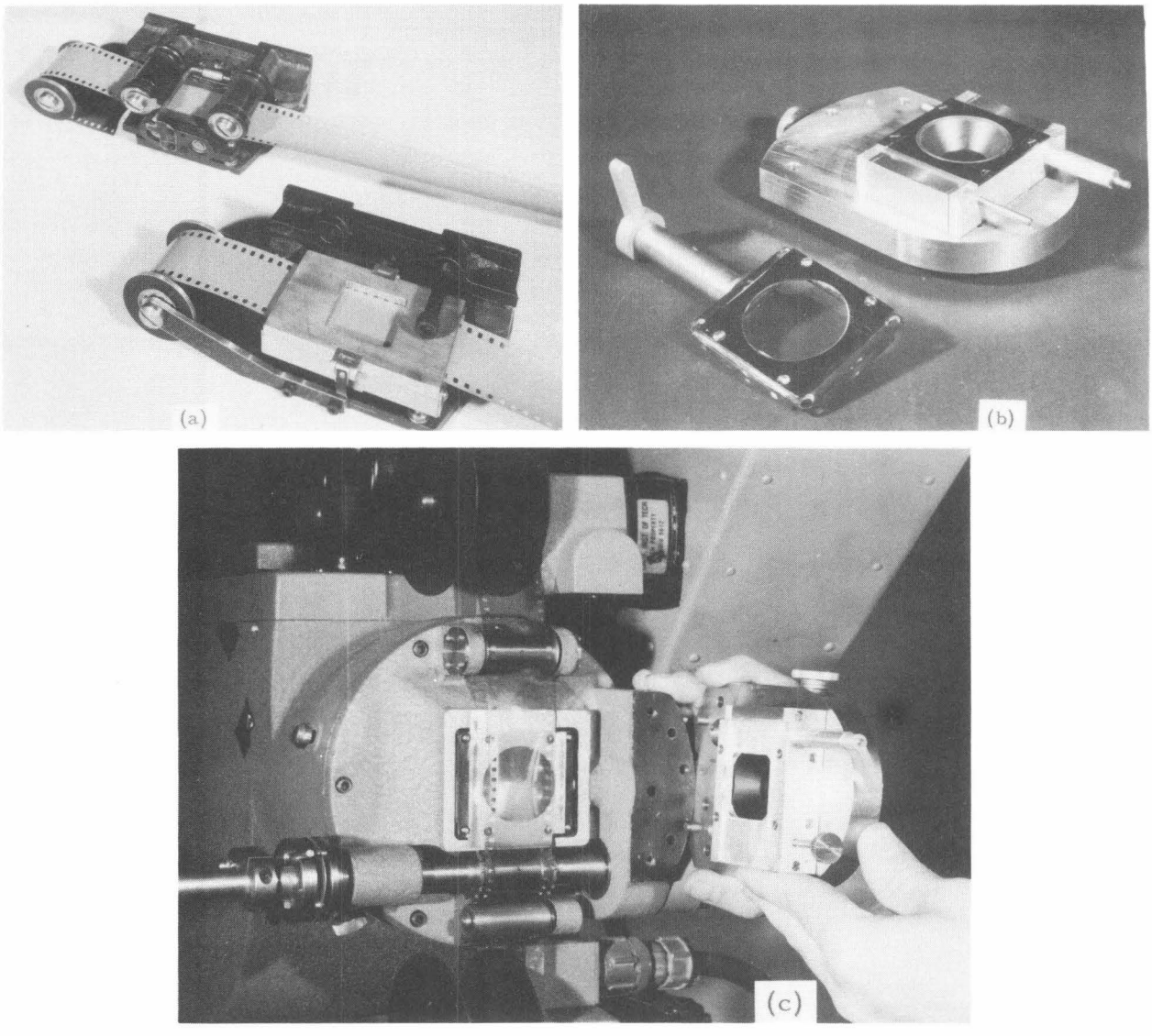

Fig. 6 - Comparison of roller and slot type camera and projector film gates: (a) camera film gates, (b) original projector gate, (c) improved projector gate.

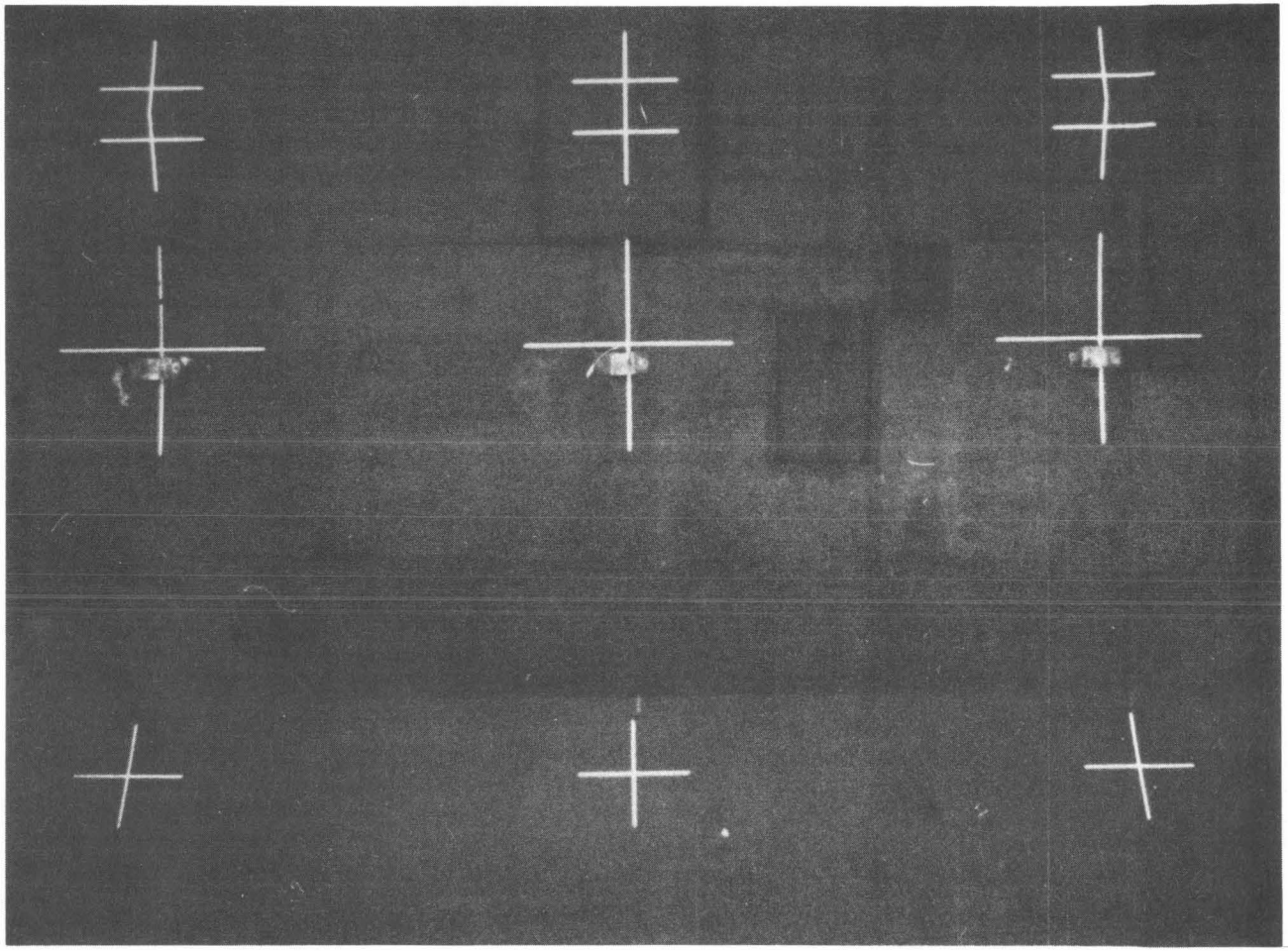

Fig.7 - Reference cross system in the Controlled Atmosphere Launching Tank as seen by Camera No. 6.

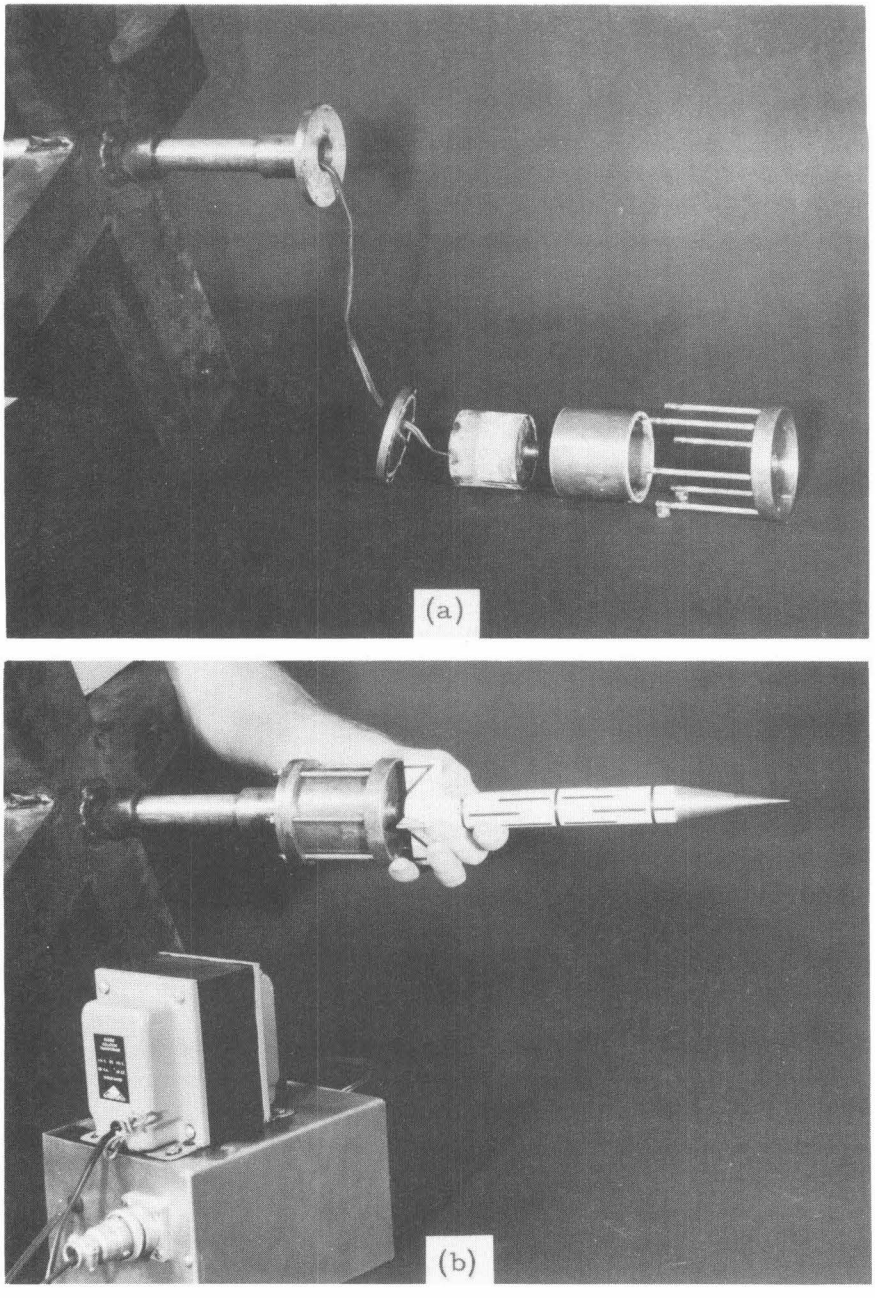

Fig. 8 - Magnetic type launcher mechanism used for vertical trajectories: (a) disassembled, (b) assembled with model in approximate location.

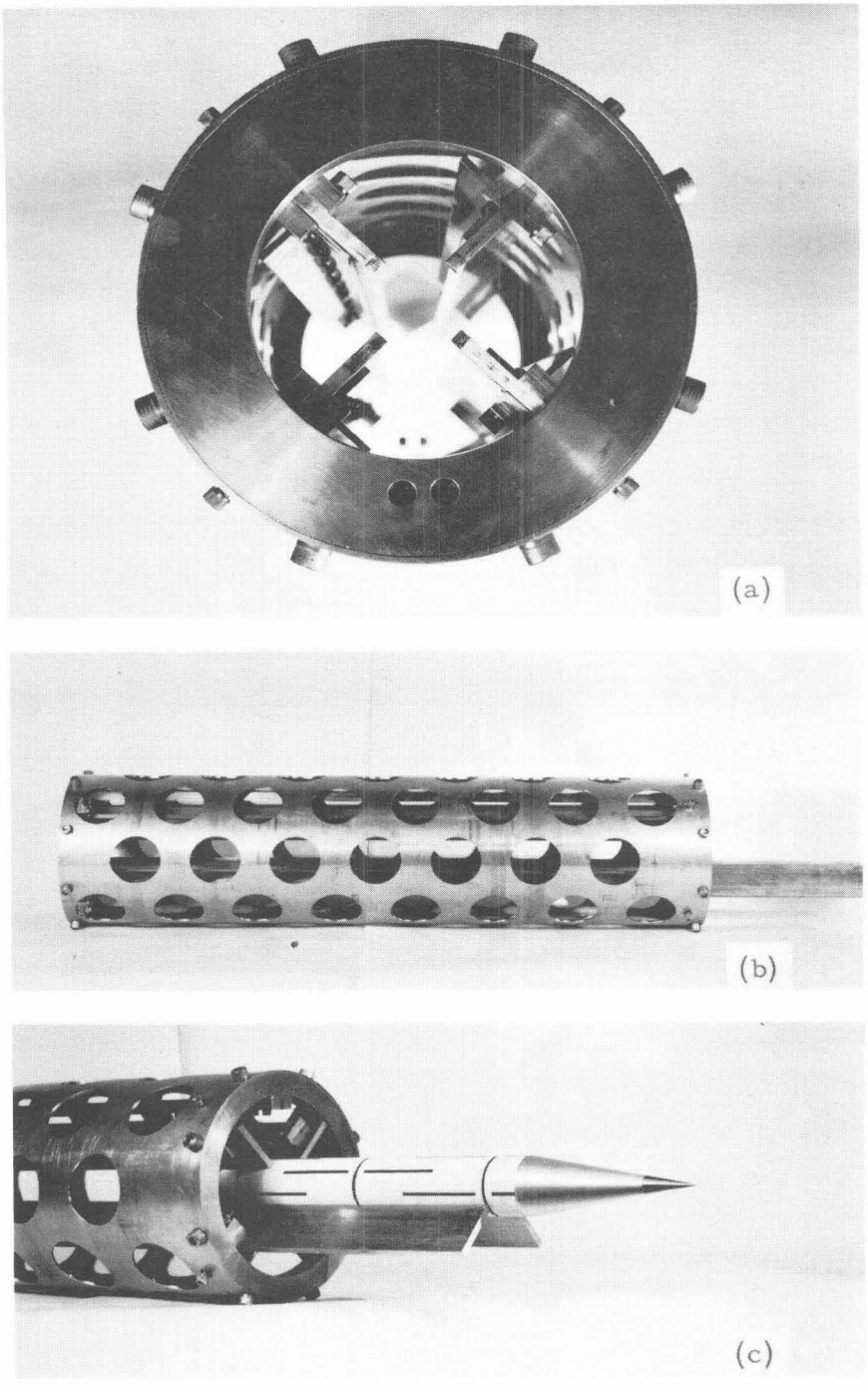

Fig. 9 - Guide rail cradle for linear launcher mechanism: (a) side view, (b) end view, (c) model position in cradle near end of acceleration stroke.

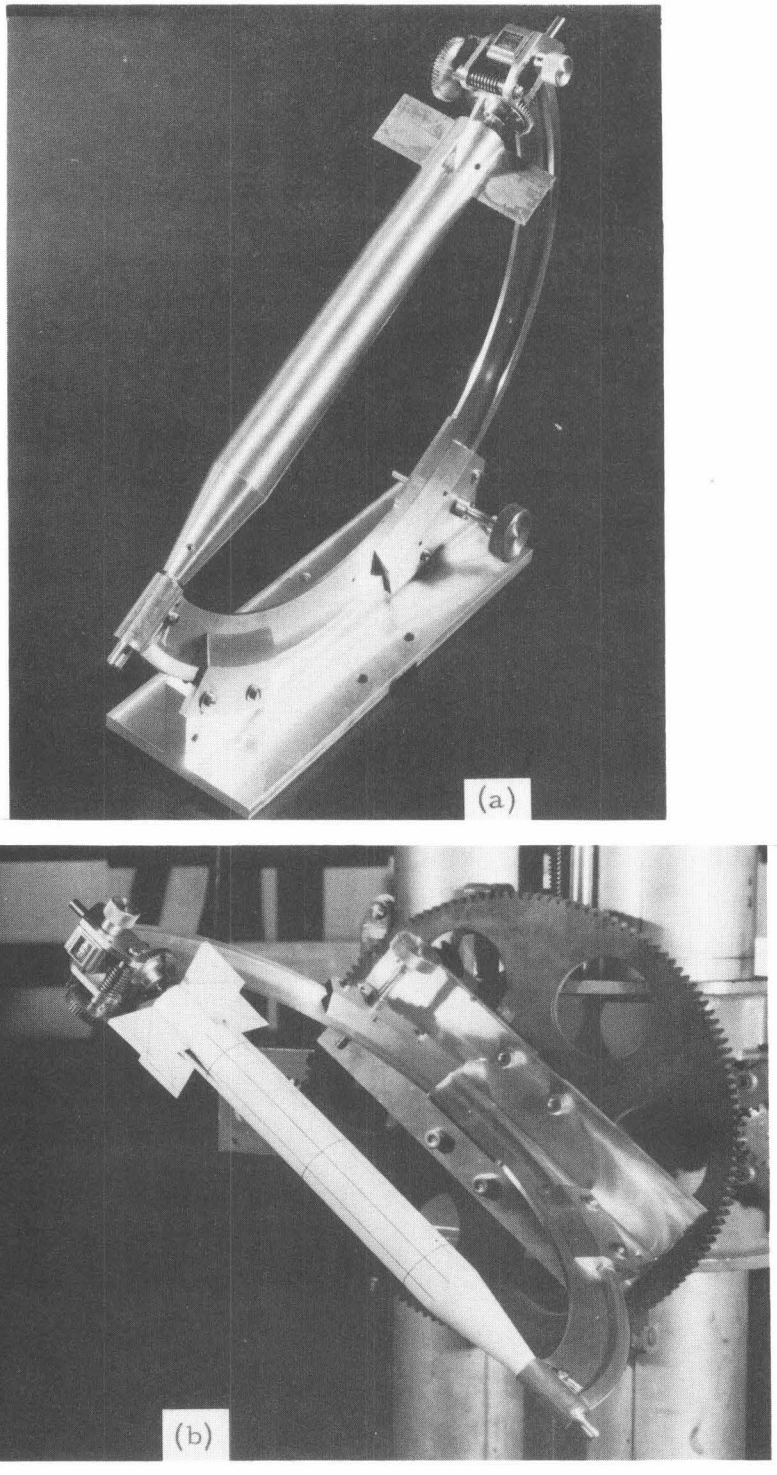

Fig. 10 - Analyzer target assembly for measuring six degrees of freedom for two-inch diameter model: (a) assembly before painting, (b) mounted on analyzer tracking mechanism.

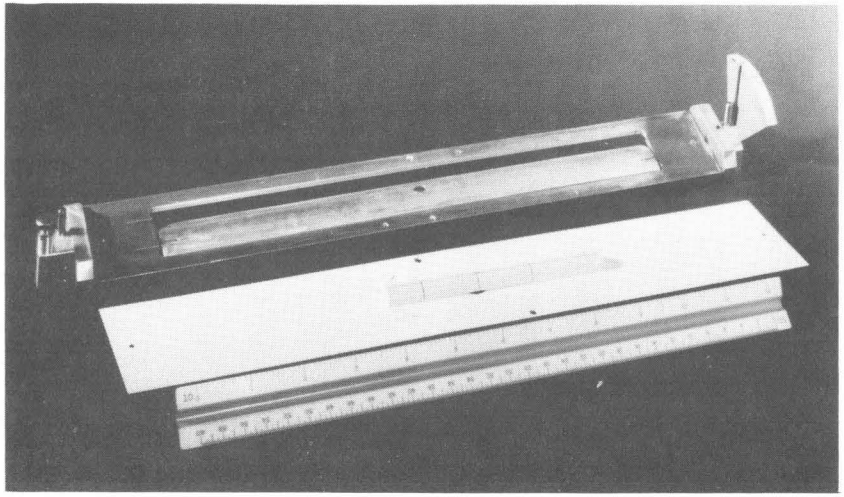

Fig. 11 - Analyzer target assembly for one-inch diameter model.

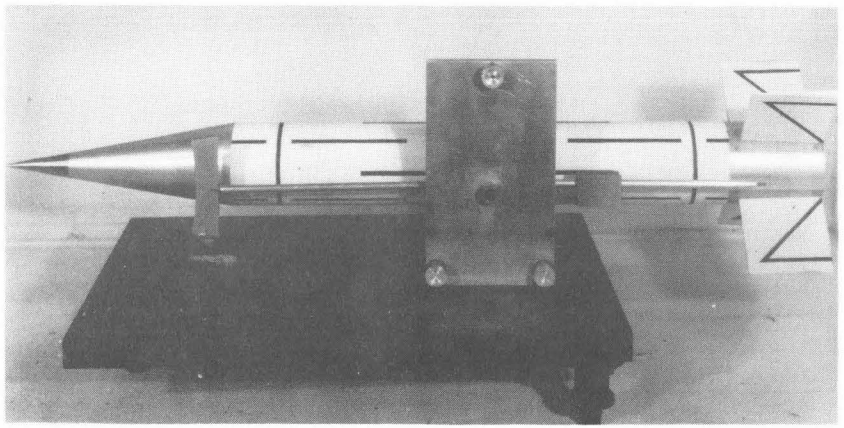

Fig. 12 - View of model and CG-I device in flotation tank for trim adjustment.

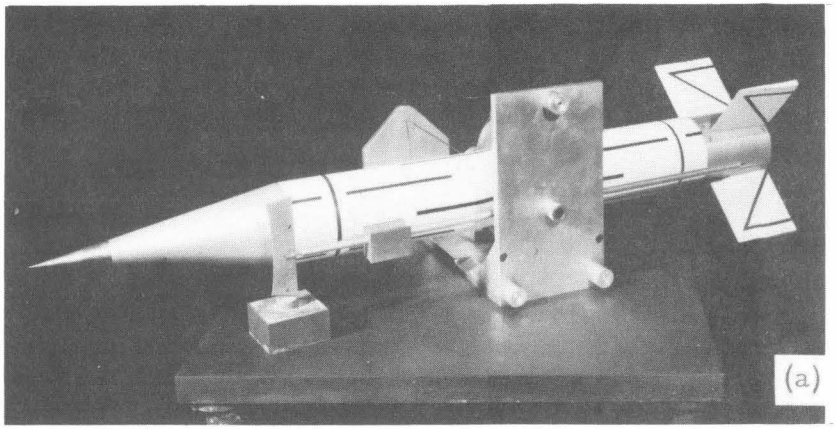

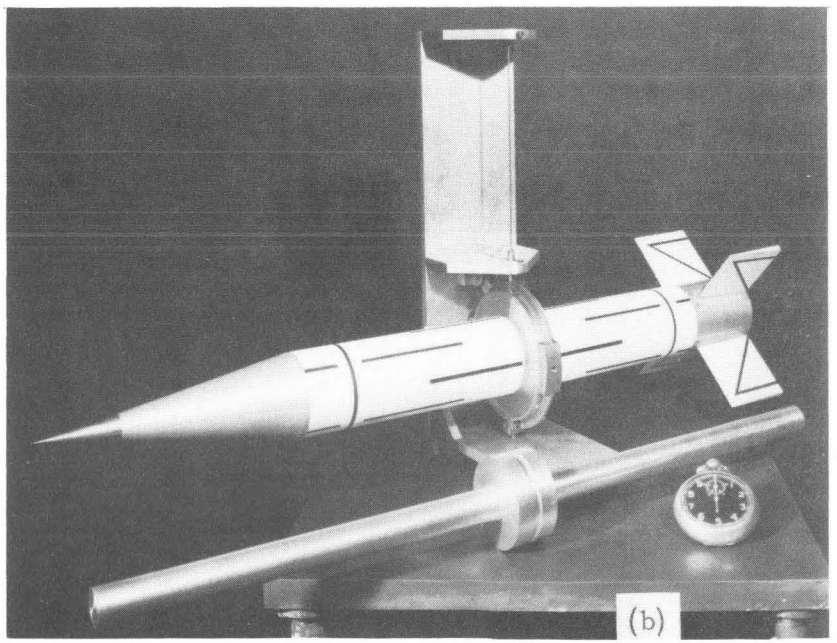

Fig. 13 - Views of model in CG-I device: (a) setup for measuring CG position, (b) setup for measuring moment of inertia.

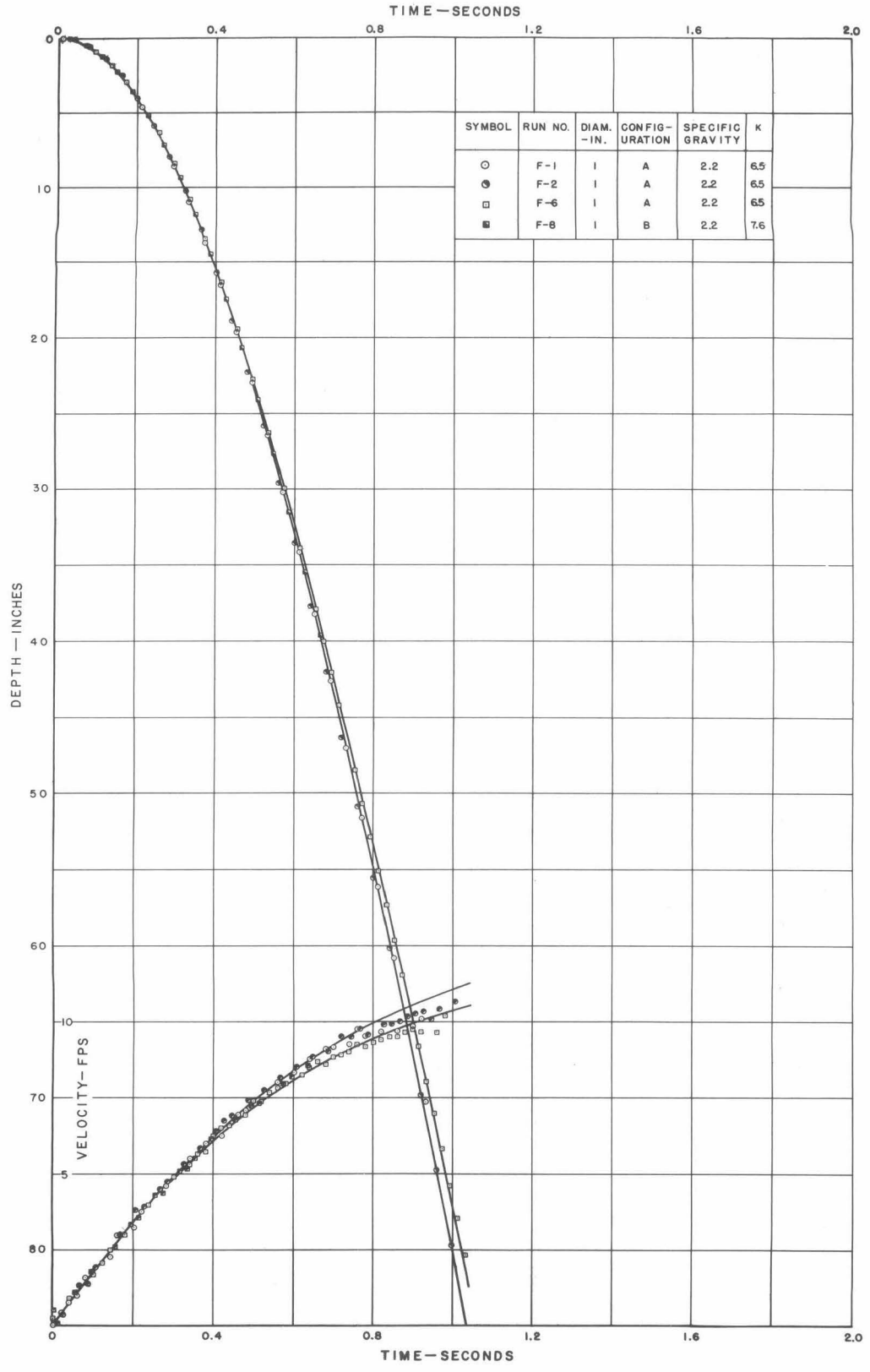

Fig. 14 - Comparison of typical experimental and computed straight vertical trajectories for the one-inch diameter model.

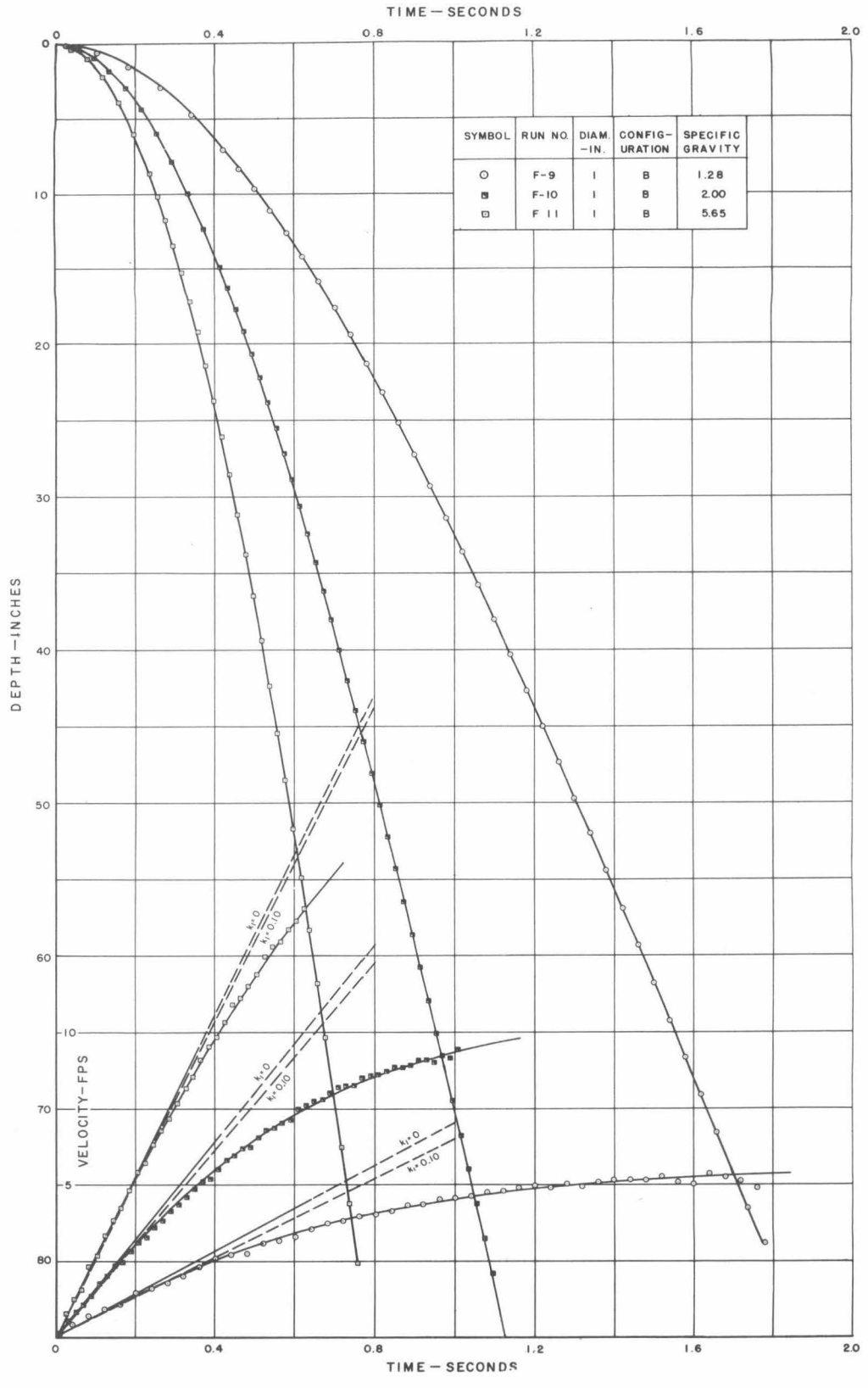

Fig. 15 - Comparison of experimental and computed straight vertical trajectories for the one-inch diameter model with variation of specific gravity.

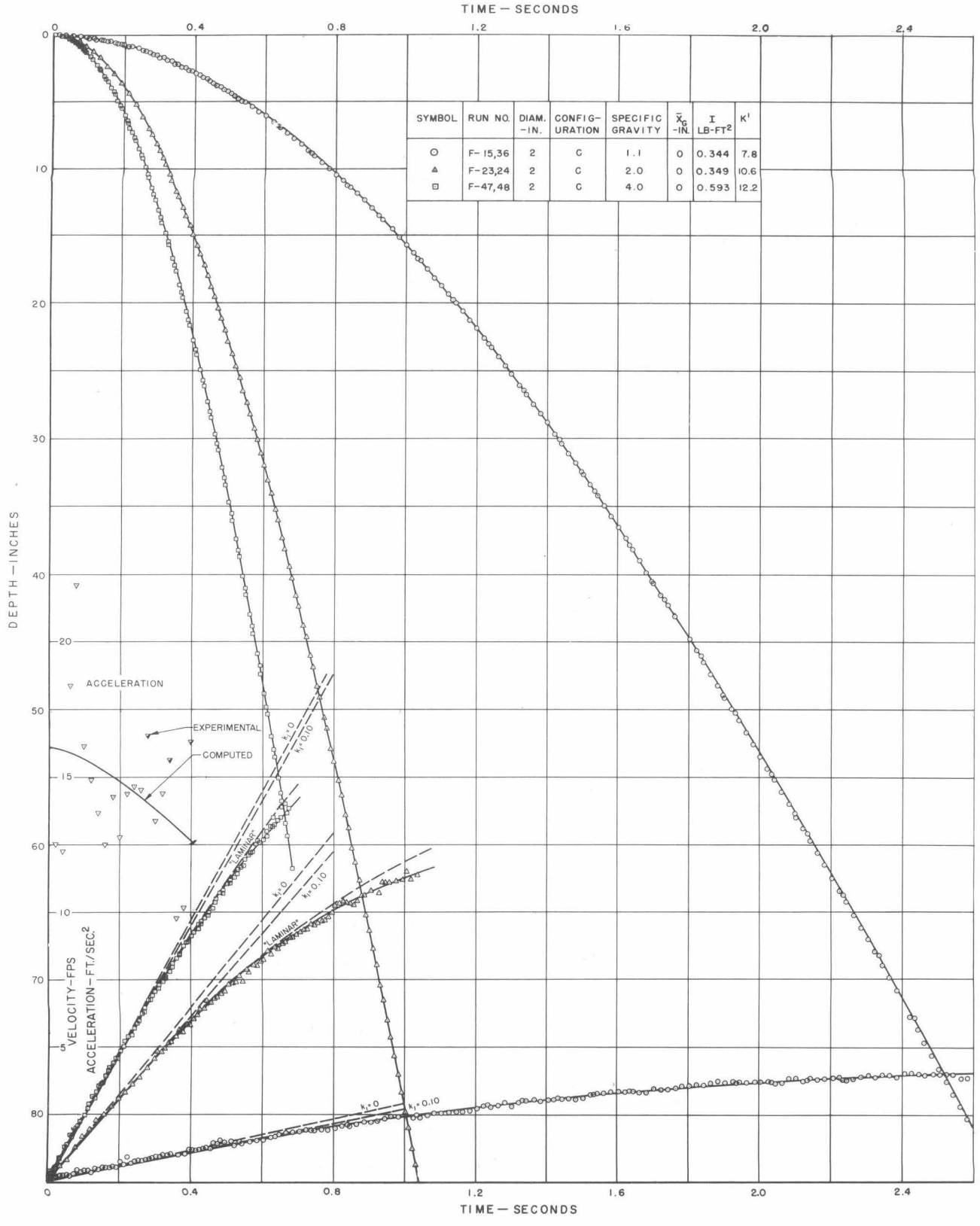

Fig. 16 - Comparison of experimental and computed straight vertical trajectories for the two-inch diameter model with variation of specific gravity.

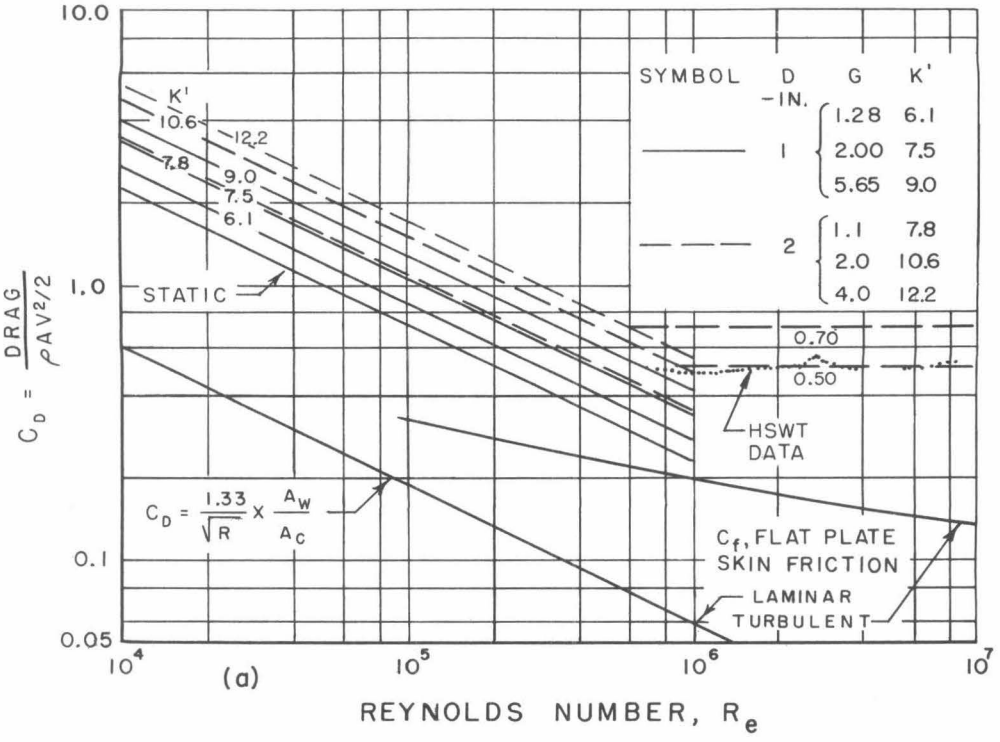

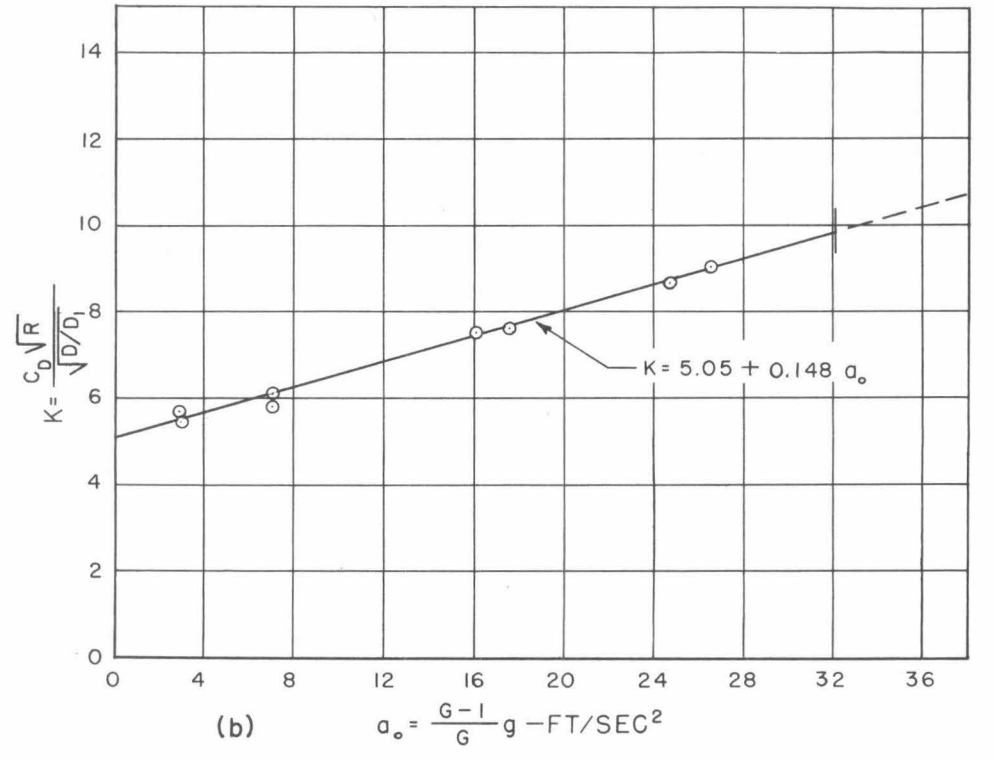

Fig. 17 - Variation of drag function with Reynolds number, model size and specific gravity: (a) drag coefficients versus Reynolds number, (b) drag parameter versus initial acceleration.

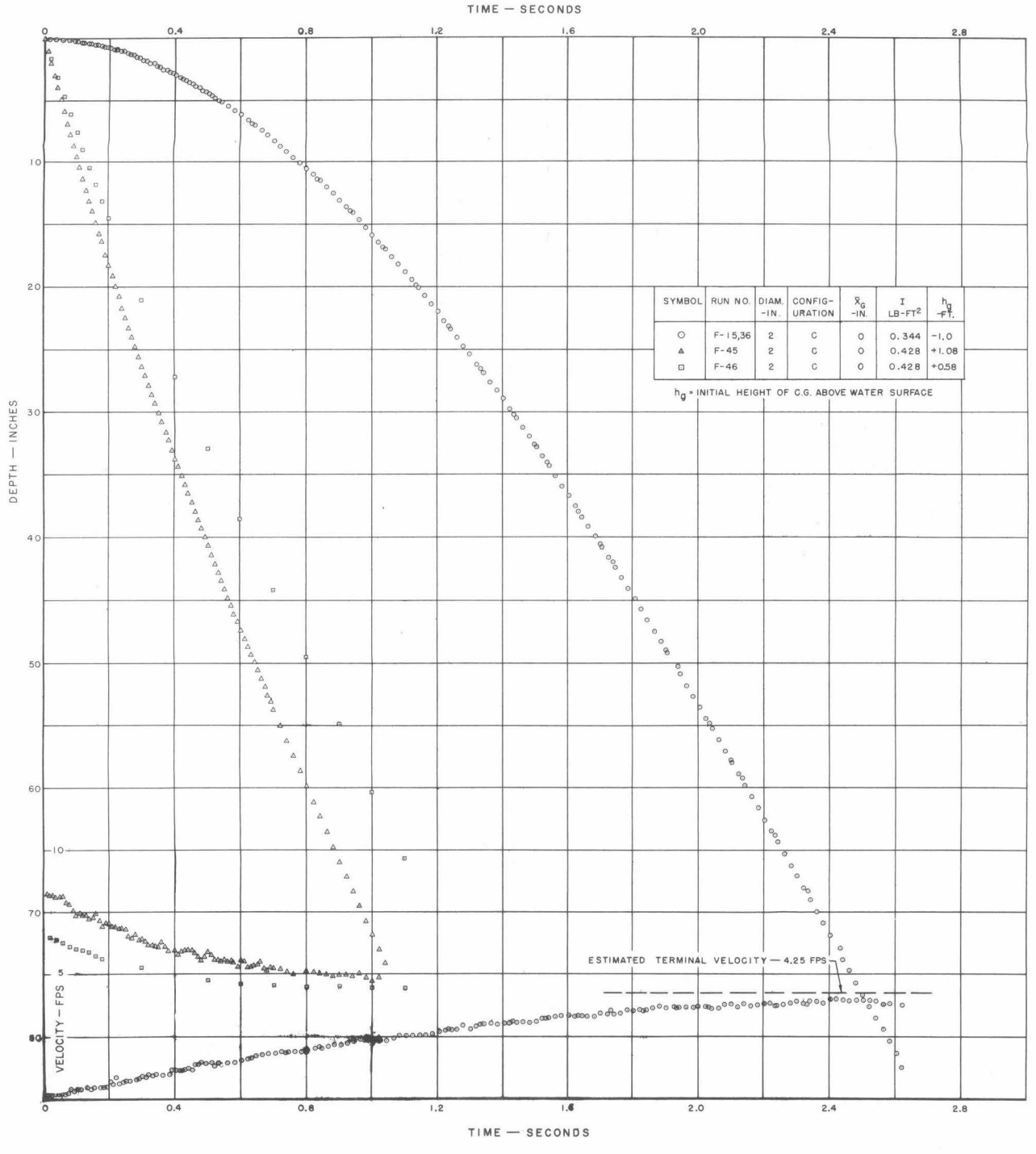

Fig. 18 - Comparison of decelerated and accelerated motion in straight vertical trajectories for the two-inch diameter model at a specific gravity of 1.1.

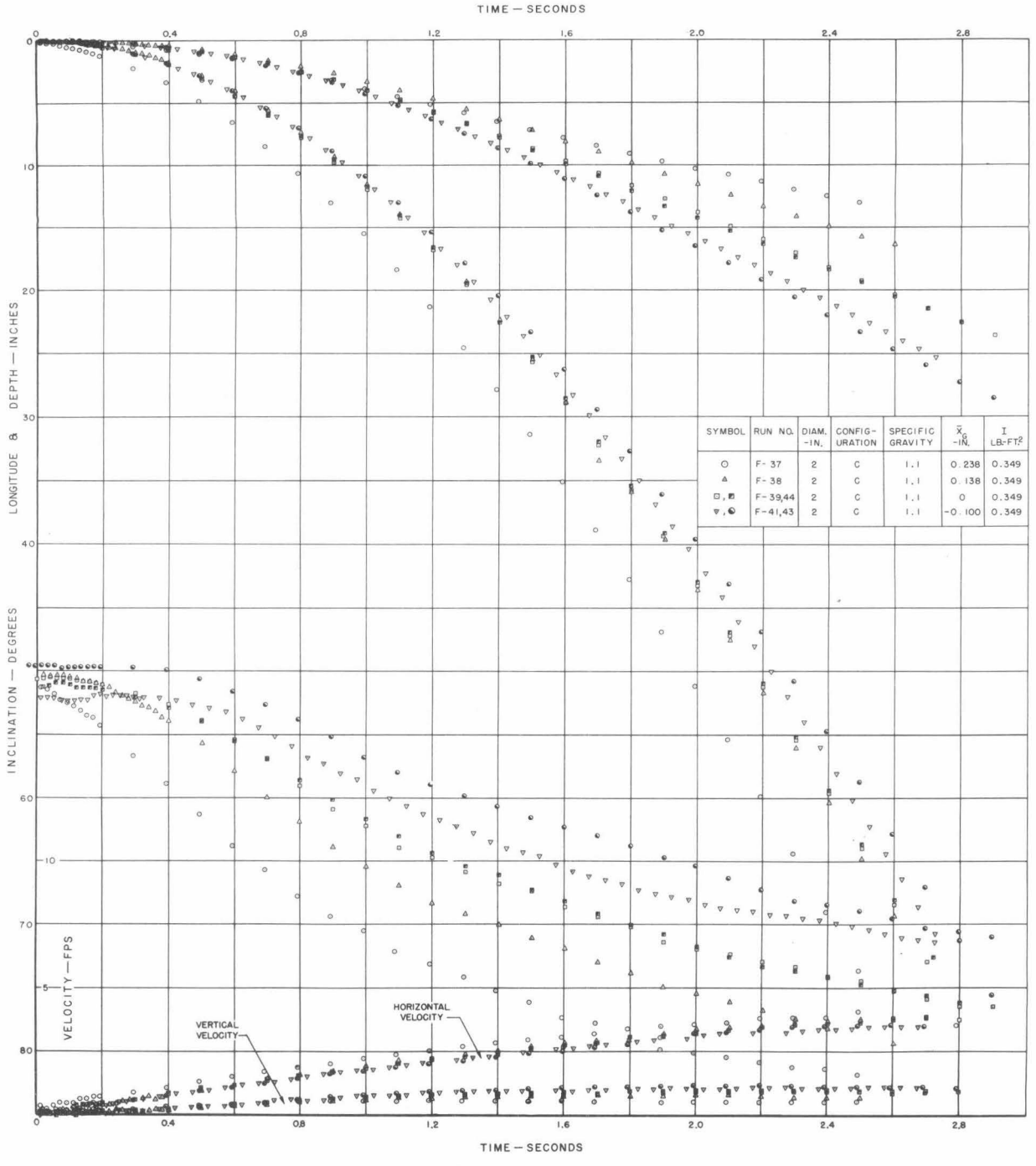

Fig. 19a - Effect of center of gravity position upon response of two-inch diameter model in curved vertical trajectories for a specific gravity of 1.1:
(a) longitude, depth, inclination and velocity versus time.

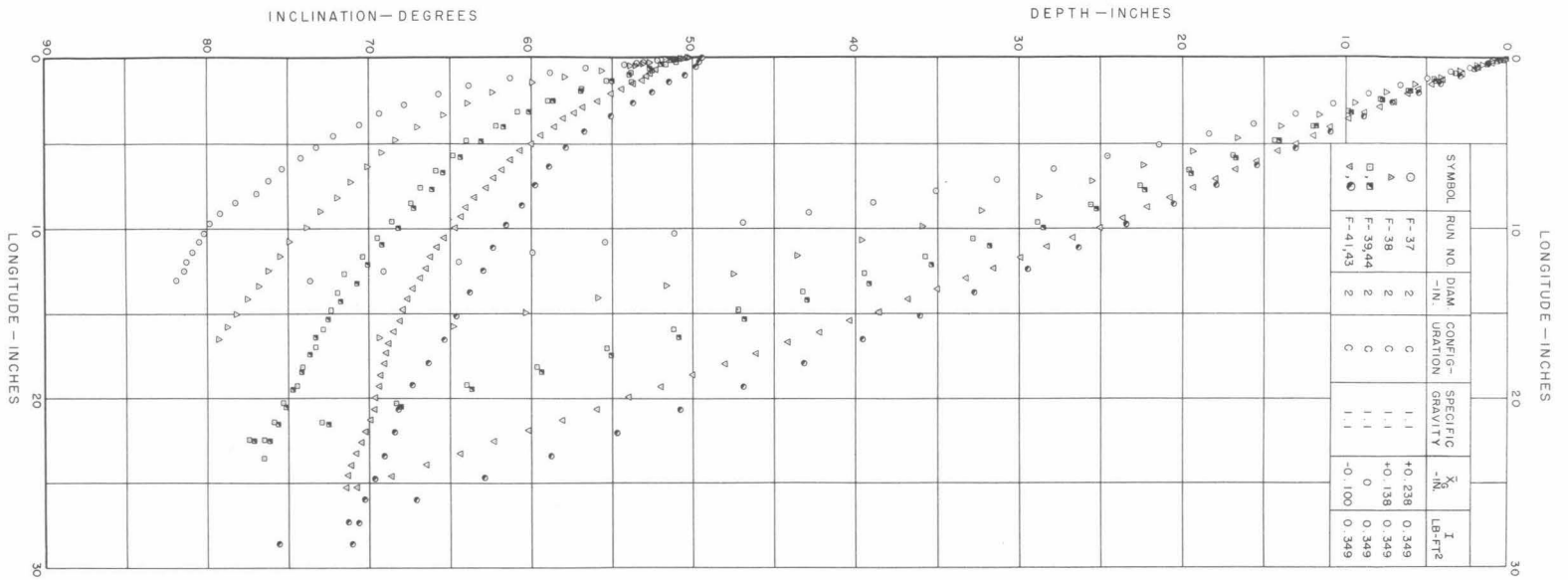

Fig. 19b - Effect of center of gravity position upon response of two-inch diameter model in curved vertical trajectories for a specific gravity of 1.1:
(b) depth, inclination and velocity versus longitude.

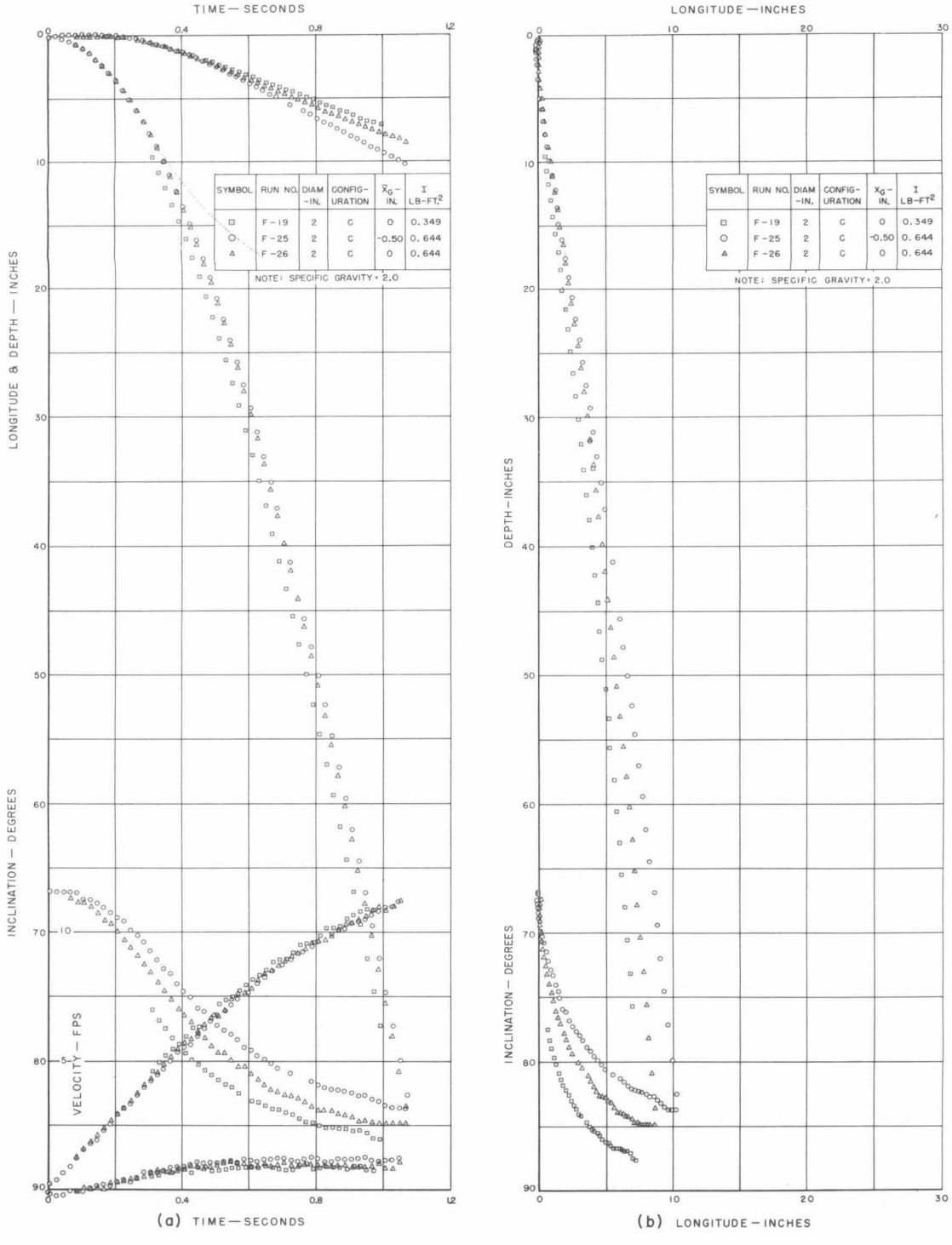

Fig. 20 - Relative effects of moment inertia increase and center of gravity shift upon response of two-inch diameter model in curved vertical trajectories: (a) longitude, depth, inclination and velocity versus time, (b) depth, inclination and velocity versus longitude.

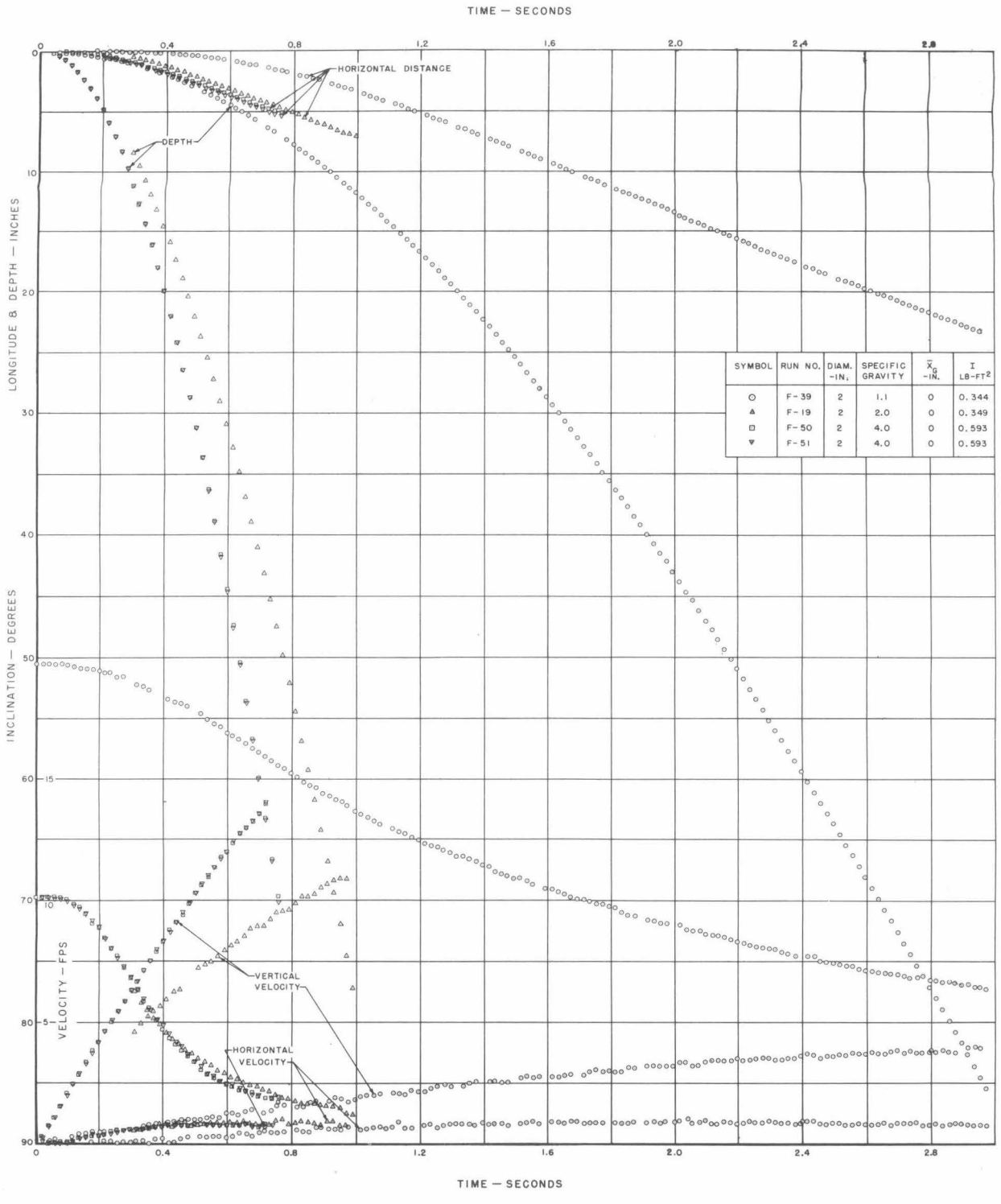

Fig. 21a - Effect of specific gravity and moment of inertia upon response of two-inch diameter model in curved vertical trajectories: (a) longitude, depth, inclination and velocity versus time.

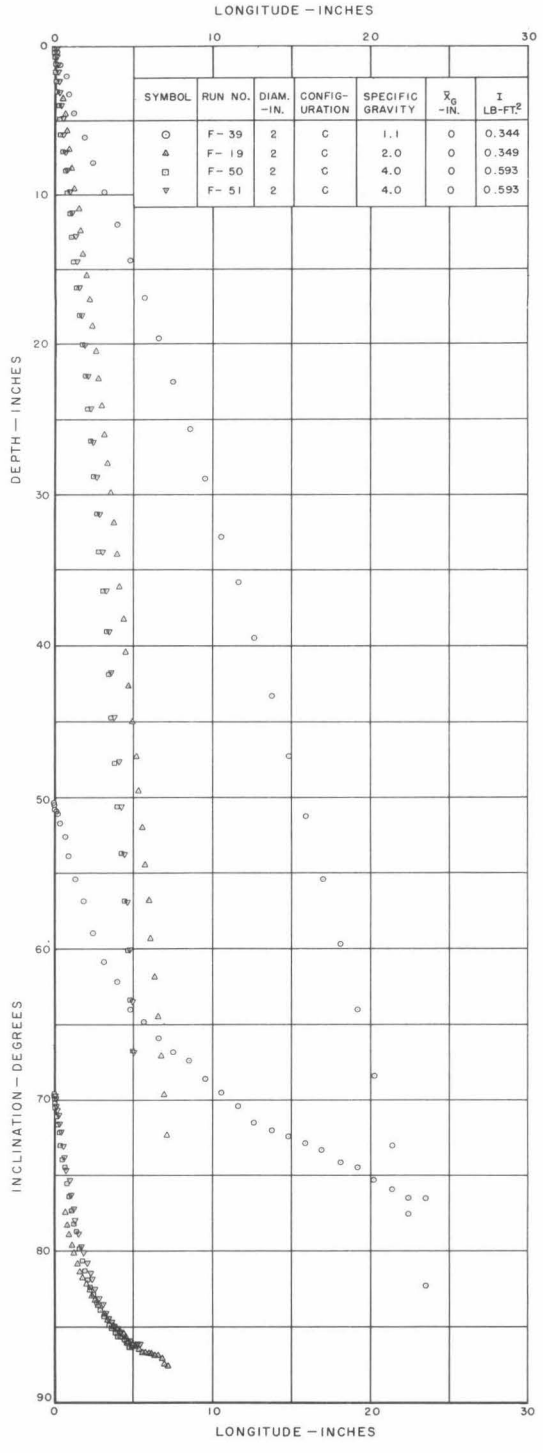

Fig. 21b - Effect of specific gravity and moment of inertia upon response of two-inch diameter model in curved vertical trajectories: (b) depth, inclination and velocity versus longitude.

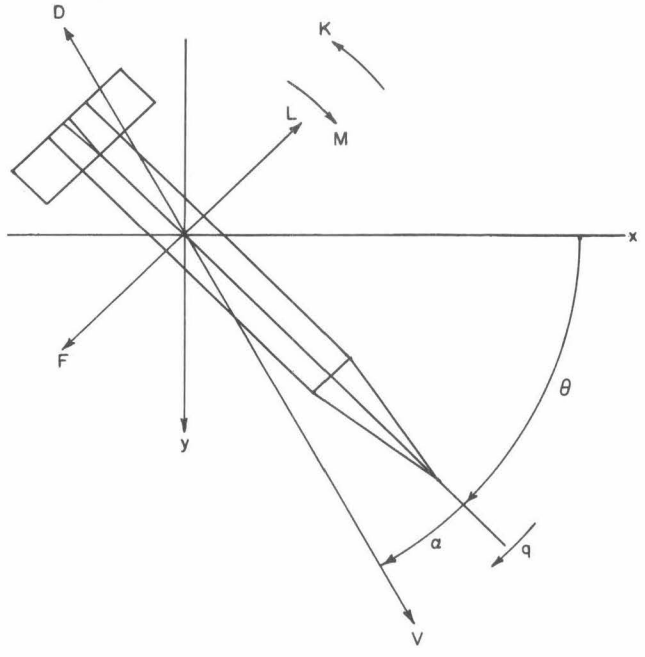

(a)

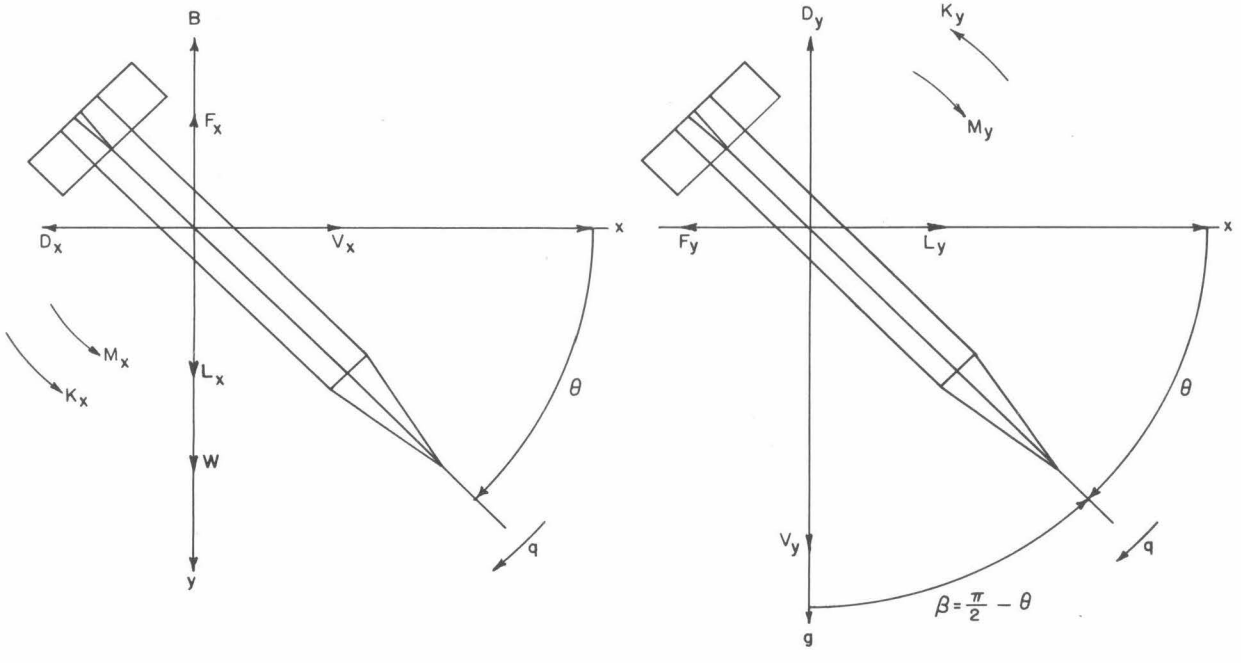

(b)

Fig. A-1 - Missile reference system: (a) force system, (b) CALT trajectory system.

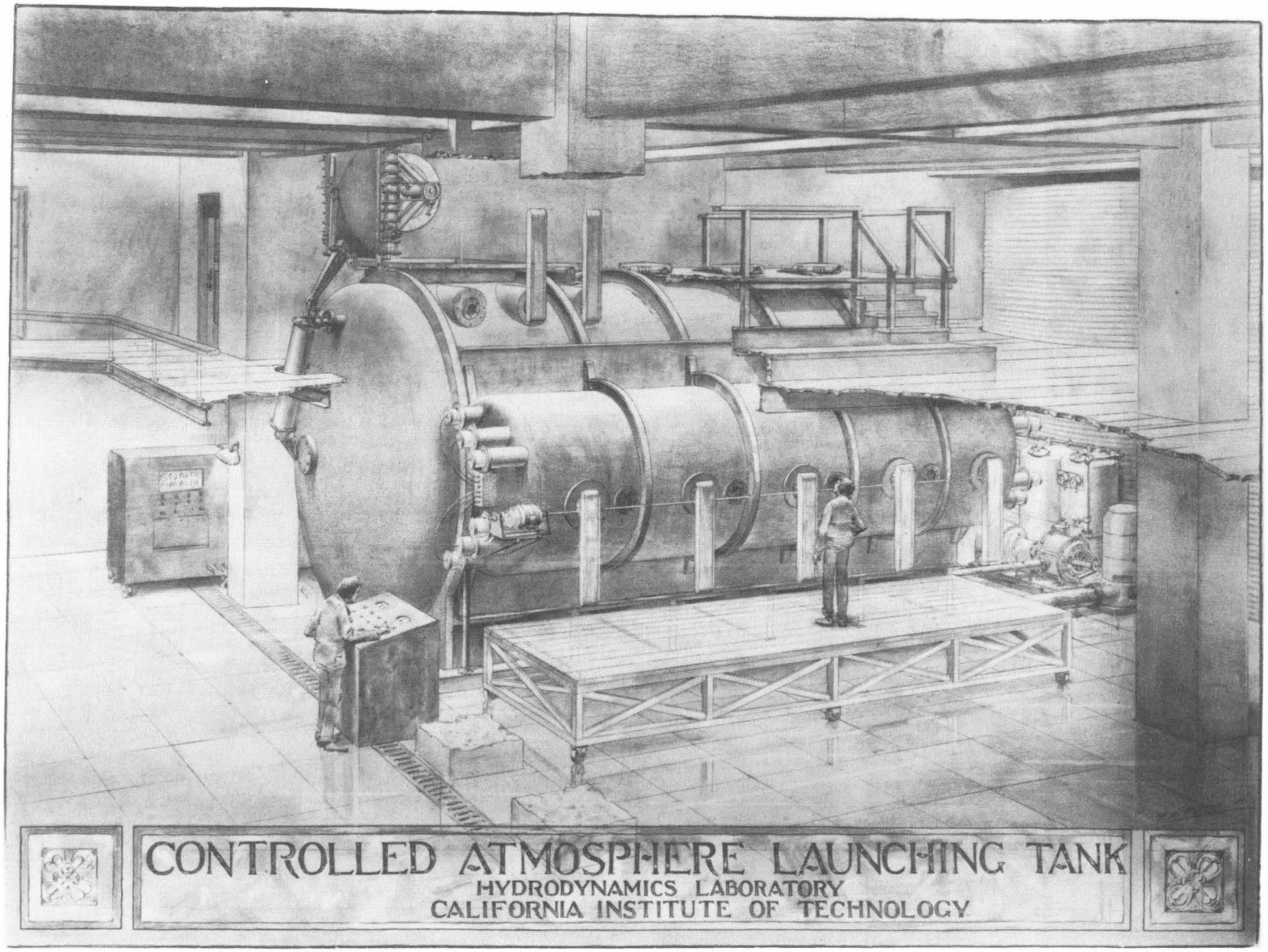

Fig. B-1 - Artist's drawing of the Controlled Atmosphere Launching Tank.

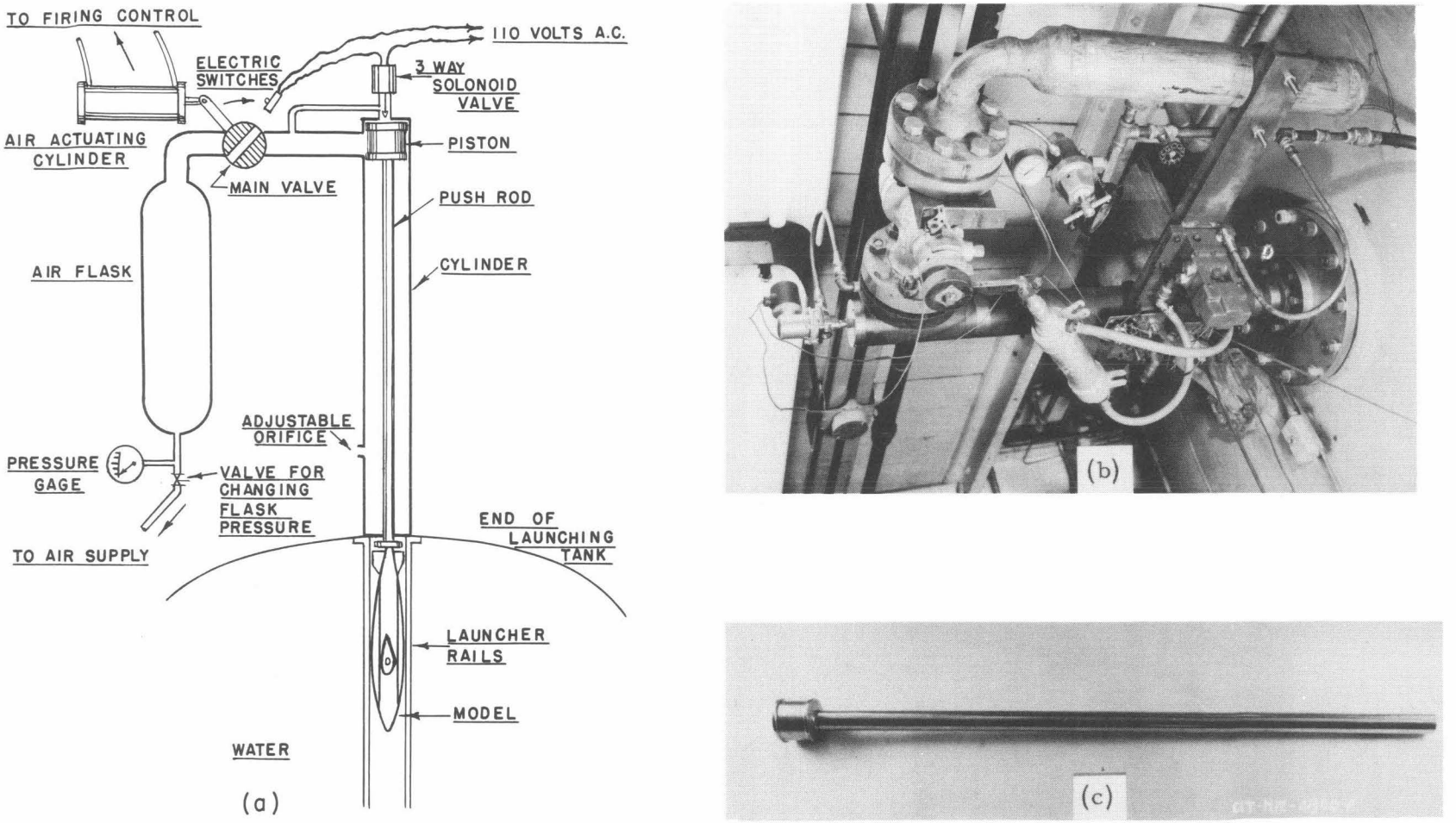

Fig. B-2 - Air-operated linear launcher mechanism: (a) schematic diagram, (b) actuating mechanism, (c) piston and rod assembly.

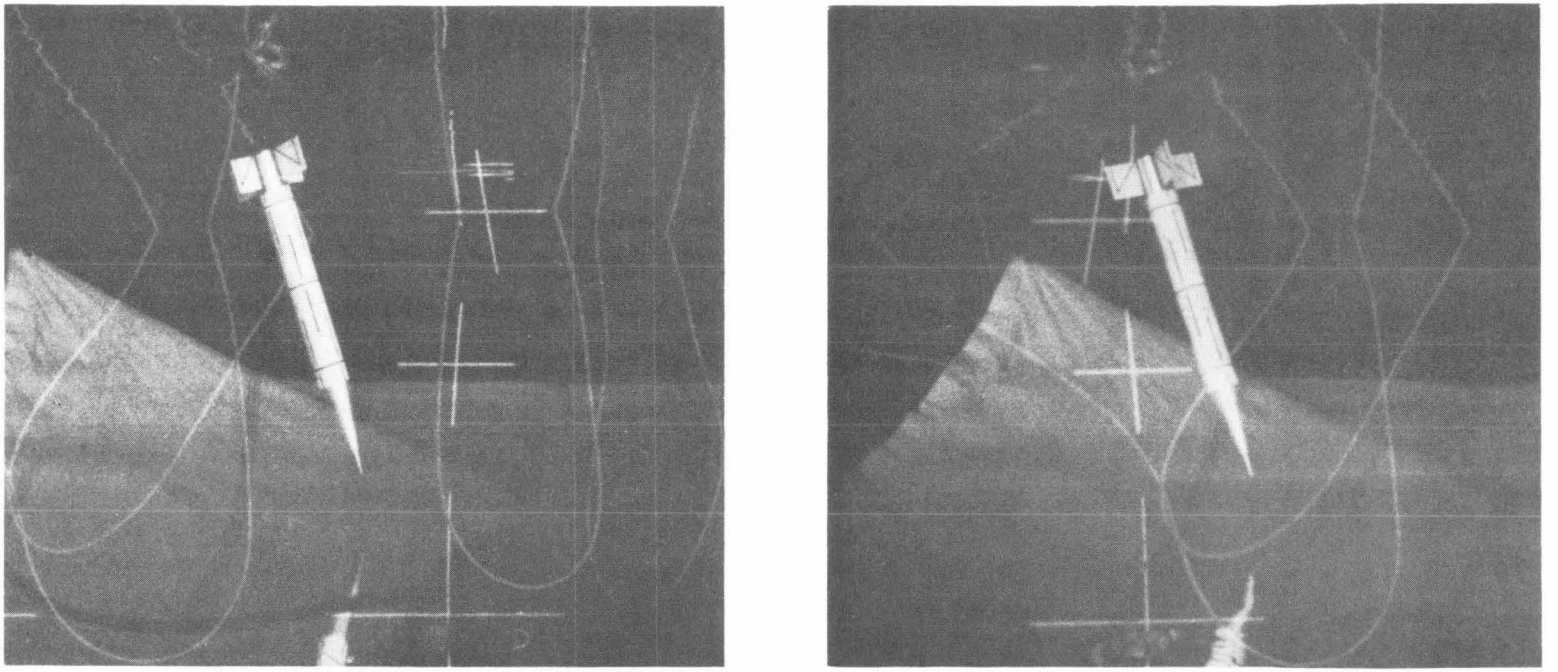

Fig. B-5 - Typical pair of simultaneous images as seen from adjacent cameras.

TABLE I

MODEL TEST PROGRAM – PART I

BASIC FINNER RESEARCH MISSILE

PHASE NO.	TEST RUN NO.	MODEL CONFIGURATION					LAUNCHING CONDITIONS		
		DIAM. – INCHES	FIN CONFIGURATION	SPECIFIC GRAVITY	C.G. POSITION – INCHES	MOMENT OF INERTIA LB–FT^2	INCLINATION – DEGREES	VELOCITY – FT/SEC	TYPE
Ia	1, 2 X	1	A	2.22	+0.1	0.0248	90	0	HAND X
	6, 8	1	A	2.20	+0.1	0.0248	90	0	HAND X
	9	1	B	1.28	+0.1	0.0200	90	0	MAGNET
	10	1	B	2.00	+0.1	N.M.	90	0	MAGNET
	11	1	B	5.65	+0.1	N.M.	90	0	MAGNET
Ia	15,36	2	C	1.10	+0.1	0.344	90	0	MAGNET
	23,24	2	C XX	2.00	+0.1	0.349	90	0	MAGNET
	47,48	2	C	4.00	+0.1	0.593	90	0	MAGNET
Ib	16,39	2	C	1.10	0	0.344	50	0	MAGNET
	40,41	2	C	1.10	-0.1	0.344	50	0	MAGNET
	44	2	C	1.10	0	0.401	50	0	MAGNET
	18,43	2	C	1.10	-0.1	0.401	50	0	MAGNET
	37,38	2	C	1.10	+0.2,+0.1	0.401	50	0	MAGNET
	19	2	C	2.00	0	0.349	70	0	MAGNET
	20,26	2	C	2.00	0	0.644	70	0	MAGNET
	21,25	2	C	2.00	−0.5	0.644	70	0	MAGNET
	22,27	2	C XX	2.00	−0.5	0.644	70	0	MAGNET
	50,51	2	C	4.00	0	0.593	70	0	MAGNET
Ic	44,45	2	C	1.10	+0.1	0.344	90	XXX	MAGNET

X TRAILING STRING

XX NOSE TIP ROUNDED

XXX MODEL SUSPENDED ABOVE WATER SURFACE

TABLE 2

MODEL PARAMETERS
BASIC FINNER RESEARCH MISSILE

DIMENSION	STANDARD CONFIGURATION	MODEL DIAMETER	
		1 IN.	2 IN.
DIAMETER — IN.	D	1.003 ± .002	2.000 $^{+.001}_{-.002}$
LENGTH — IN.	10 D	9.998	19.985 (19.738)*
FIN CHORD — IN.	D	1.000 ± .002	2.002 ± .001
FIN SPAN — IN.	3 D	2.998	6.002 ± .002
TRAILING EDGE THICKNESS — IN.	0.08 D PLUS L.E. THICKNESS	0.062	0.172 ± .001
LEADING EDGE THICKNESS — IN.	0	0.004	0.010 ± .002
NOSE CONE ANGLE — DEG.	20	19.9	20.2
NOSE TIP RADIUS — IN.	0	0.005	0.005
SURFACE AREA — FT.^{2}	0.343 D	0.343	0.974
BUOYANCY — LBS.	0.236 D^3	0.240	1.885
WEIGHT — LBS.	—	0.313 — 1.359	1.268 — 9.425
SPECIFIC GRAVITY	—	1.30 — 5.67	0.87 — 5.00
LONGITUDINAL C.B. (IN. FORWARD OF BASE)	3.95 D	3.98	7.955
LONGITUDINAL C.G. (IN. FORWARD OF BASE)			
S P. G R. = 1	—	—	6.6 — 9.0
S P. G R. = 2	—	2.75 — 4.38	5.2 — 10.1
MOMENT OF INERTIA - LB-FT^2			
S P. G R. = 1	—	0.0202	0.34 — 0.40
S P. G R. = 2	—	0.0248	0.35 — 0.65

*NOSE TIP ROUNDED

TABLE 3 - TIME-POSITION DATA FOR PHASE 1a
STRAIGHT VERTICAL TRAJECTORIES

Depth - Inches											
Time Secs.	F-9	F-10	F-11	F-15 d_o = - 0.04	F-23 d_o = - 8.18	F-24	F-36	F-45	F-46 Released above water surface	F-47	F-48
t_o	0	0	0	0.06	-0.28	0	+0.06	-	-	0	0
0	0	0	0	0	0	0	0	0	0	0	0
0.02		0.02	0.02	0.14	1.14	0.02	0	1.000		.080	0
0.04	0.06	0.14	0.09	0.23	2.29	0.14	0	1.978	1.572	.278	0.09
0.06		0.34	0.27	0.32	3.46	0.27	0.01	2.956		.598	0.40
0.08	0.25	0.59	0.56	0.39	4.74	0.51	0.01	3.932	3.112	1.074	0.72
0.10		0.91	0.92	0.49	6.13	0.89	0.05	4.892		1.600	1.19
0.12	0.57	1.32	1.47	0.65	7.51	1.31	0.12	5.876	4.632	2.284	1.80
0.14		1.80	2.10	0.74	9.00	1.82	0.17	6.846		3.078	2.49
0.16	1.00	2.35	2.91	0.96	10.54	2.40	0.24	7.768	6.092	3.946	3.30
0.18		2.93	3.82	1.14	12.18	3.01	0.31	8.718		4.952	4.23
0.20	1.50	3.60	4.82	1.32	13.77	3.73	0.42	9.576	7.570	6.042	5.27
0.22		4.34	5.96	1.52	15.50	4.47	0.52	10.482		7.278	6.43
0.24	2.20	5.12	7.25	1.72	17.26	5.30	0.65	11.368	8.992	8.570	7.65
0.26		5.98	8.61	1.96	19.05	6.21	0.78	12.248		9.988	9.00
0.28	2.95	6.88	10.11	2.21	20.81	7.16	0.89	13.132	10.426	11.522	10.46
0.30		7.87	11.73	2.45	22.71	8.23	1.04	13.978		13.160	12.00
0.32	3.80	8.90	13.44	2.67	24.63	9.33	1.19	14.876	11.818	14.894	13.70
0.34		9.99	15.27	2.94	26.64	10.50	1.37	15.768		16.736	15.43
0.36	4.74	11.15	17.22	3.23	28.67	11.78	1.58	16.396	13.182	18.648	17.28
0.38		12.36	19.26	3.51	30.77	13.08	1.80	17.426		20.658	19.24
0.40	5.84	13.60	21.43	3.82	32.91	14.41	2.03	18.288	14.508	22.776	21.30
0.42		14.91	23.71	4.15	35.09	15.85	2.28	19.106		24.986	23.47
0.44	7.07	16.29	26.07	4.46	37.32	17.36	2.52	19.942		27.320	25.73
0.46		17.71	28.55	4.79	39.56	18.90	2.80	20.766		29.710	28.04
0.48	8.35	19.19	31.15	5.12	41.86	20.52	3.08	21.580		32.218	30.46
0.50		20.68	33.81	5.46	44.16	22.17	3.35	22.408		34.790	33.00
0.52	9.66	22.25	36.56	5.81	46.54	23.86	3.64	23.212		37.458	35.59
0.54		23.87	39.40	6.17		25.67	3.95	23.956		40.226	38.29
0.56	11.13	25.51	42.38	6.56		27.51	4.30	24.760		43.076	41.05
0.58		27.20	45.44	6.97		29.42	4.66	25.532		45.980	43.90
0.60	12.62	28.90	48.54	7.39		31.33	5.01	26.286	21.058	49.002	46.89
0.62		30.69	51.74	7.81		33.33		27.066		52.128	49.96
0.64	14.18	32.51	55.00	8.25		35.41		27.802		55.250	53.06
0.66		34.36	58.35	8.70		37.47		28.546		58.562	56.26
0.68	15.87	36.23	61.83	9.16		39.59		29.282			59.50
0.70		38.14	65.36	9.61		41.77	6.84	30.016			62.80
0.72	17.65	40.11	68.93	10.07		43.96		30.740			
0.74		42.09	72.60	10.53		46.22		31.528			
0.76	19.46	44.06	76.33	10.99		48.50		32.202			
0.78		46.10	80.18	11.47		50.77		32.952			
0.80	21.34	48.16		11.97		53.11	8.97	33.700	27.176		
0.82		50.22		12.49		55.54		34.384			
0.84	23.25	52.31		13.02		58.04		35.082			
0.86		54.43		13.54		60.47		35.798			
0.88	25.21	56.55		14.10		62.95		36.514			
0.90		58.69		14.66		65.47	11.36	37.228			
0.92	27.26	60.86		15.26		68.01		37.938			
0.94		63.04		15.83		70.66		38.630			
0.96	29.33	65.20		16.40		73.31		39.308			
0.98		67.41		16.96		75.96		39.968			
1.00	31.50	69.61		17.58		78.65	13.95	40.676	32.998		
1.10	37.00	80.92		20.68			16.81	44.056			
1.20	42.74			24.02			19.86	47.358	38.648		
1.30	48.61			27.59			23.14	50.580			
1.40	54.57			31.24			26.59	53.772	44.180		
1.50	60.69			35.09			30.23				
1.60	66.82			39.11			33.99	59.944	49.590		
1.70				43.20			37.93				
1.80							41.95	65.906	54.940		
1.90							46.13				
2.00							50.45	71.840	60.356		
2.10							54.85				
2.20							59.30		65.704		
2.30							63.82				
2.40							68.36		70.960		
2.50							72.96				

TABLE 4 - TIME-POSITION DATA FOR PHASE 1b - CURVED VERTICAL TRAJECTORIES

Time Secs.	F-39 Depth in.	F-39 Long. in.	F-39 Incl. deg.	F-41 Depth in.	F-41 Long. in.	F-41 Incl. deg.	F-43 Depth in.	F-43 Long. in.	F-43 Incl. deg.	F-44 Depth in.	F-44 Long. in.	F-44 Incl. deg.	F-50 Depth in.	F-50 Long. in.	F-50 Incl. deg.	F-51 Depth in.	F-51 Long. in.	F-51 Incl. deg.
	d_o=0	L_o=0	Θ_o=50.6	d_o=0	L_o=0	Θ_o=52.0	d_o=0	L_o=0	Θ_o=49.6	d_o=0	L_o=0	Θ_o=51.3	d_o=0	L_o=0	Θ_o=69.7	d_o=0	L_o=0	Θ_o=69.6
t_o	0			+0.03			+0.01			0			0			0		
0	0	0	50.6	0.02	0	52.0	0	0	49.6	0	0	51.3	0.01	-0.01	69.7	0	0	69.6
0.02	-0.01	0.02	50.4	0.04	-0.01	52.0	-0.01	-0.03	49.5	-0.02	0.01	51.2	0.02	-0.03	69.7	0.04	0.07	69.6
0.04	0.01	0.09	50.5	0.06	-0.04	52.0	0.03	0.01	49.5	0.01	0.05	51.1	0.16	-0.02	69.6	0.14	0.07	69.7
0.06	0.05	0.08	50.5	0.07	-0.03	52.0	0	0.02	49.5	0.03	0.03	50.9	0.39	-0.01	69.7	0.37	0.11	69.8
0.08	0.10	0.07	50.5	0.08	-0.03	52.1	0.06	0.02	49.7	0.06	0.03	50.9	0.68	0	69.7	0.71	0.09	69.8
.10	0.12	0.09	50.5	0.08	0.01	52.2	0.09	0.03	49.6	0.06	0.09	51.1	1.13	0.03	69.9	1.12	0.12	70.0
.12	0.14	0.12	50.8	0.12	0.02	52.2	0.12	0.03	49.6	0.15	0.08	51.3	1.69	0.04	70.2	1.68	0.14	70.3
.14	0.29	0.14	50.8	0.20	0.02	52.2	0.21	0.03	49.6	0.25	0.08	51.3	2.32	0.07	70.5	2.31	0.20	70.6
.16	0.37	0.18	50.8	0.25	0.08	52.2	0.24	0.06	49.6	0.36	0.10	51.3	3.07	0.15	71.1	3.07	0.24	70.9
.18	0.43	0.17	50.9	0.29	0.09	52.2	0.38	0.07	49.6	0.46	0.13	51.3	3.93	0.22	71.7	3.90	0.34	71.5
.20	0.53	0.23	51.1	0.37	0.08	51.8	0.46	0.10	49.6	0.51	0.15	51.5	4.85	0.29	72.2	4.87	0.44	72.1
.22				0.46	0.10	51.7							5.95	0.38	73.0	5.90	0.52	73.0
.24				0.55	0.14	51.9							7.10	0.49	73.9	7.10	0.64	73.8
.26				0.63	0.15	51.8							8.37	0.62	74.5	8.36	0.75	74.6
.28				0.76	0.18	51.8							9.73	0.78	75.5	9.73	0.90	75.3
.30	1.20	0.39	51.7	0.88	0.25	51.9	1.04	0.27	49.6	1.18	0.32	52.0	11.22	0.90	76.4	11.19	1.05	76.2
.32													12.78	1.07	77.3	12.77	1.22	77.1
.34													14.43	1.21	78.3	14.42	1.37	77.9
.36													16.22	1.38	78.8	16.20	1.54	78.8
.38													18.06	1.54	79.9	18.05	1.73	79.6
.40	2.00	0.74	52.6	1.64	.46	52.1	1.82	0.57	49.9	2.00	0.60	52.8	20.01	1.72	80.6	20.05	1.89	80.1
.42													22.08	1.90	81.3	22.08	2.10	80.8
.44													24.24	2.10	81.9	24.22	2.31	81.4
.46													26.47	2.29	82.4	26.48	2.47	81.8
.48													28.77	2.47	82.8	28.80	2.67	82.5
.50	3.20	0.95	53.9	2.67	.82	52.6	2.86	1.02	50.6	3.13	0.93	54.0	31.23	2.65	83.3	31.23	2.85	83.1
.52													33.73	2.86	83.9	33.75	3.08	83.4
.54													36.34	3.05	84.3	36.37	3.27	84.1
.56													39.01	3.26	84.6	39.05	3.46	84.3
.58													41.80	3.44	84.8	41.79	3.66	84.7
.60	4.49	1.39	55.4	3.87	1.27	53.2	4.07	1.45	51.5	4.46	1.36	55.5	44.68	3.63	85.1	44.67	3.85	84.9
.62													47.59	3.82	85.4	47.59	4.06	85.0
.64													50.62	4.01	85.6	50.65	4.25	85.3
.66													53.72	4.22	85.6	53.74	4.47	85.6
.68													56.88	4.43	85.8	56.89	4.65	85.8
.70	6.07	1.91	56.9	5.33	1.78	54.4	5.42	2.01	52.6	5.96	1.92	56.9	60.09	4.61	86.1	60.10	4.82	85.8
.72													63.42	4.79	86.3	63.43	5.01	86.2
.74													66.80	4.97	86.4	66.84	5.23	86.1
.76													69.92	5.08	87.6	70.21	5.40	86.0
.78																		
.80	7.80	2.53	59.0	6.90	2.51	55.9	7.03	2.62	53.8	7.72	2.53	58.6						
.82																		
.84																		
.86																		
.88																		
.90	9.79	3.24	60.8	8.76	3.21	57.3	8.85	3.41	55.2	9.66	3.23	60.1						
.92																		
.94																		
.96																		
.98																		
1.00	11.98	4.01	62.2	10.83	4.05	58.5	10.89	4.32	56.8	11.77	4.02	61.7						
1.05																		
1.10	14.31	4.86	64.0	13.00	5.03	60.0	13.03	5.29	57.9	14.16	4.90	63.1						
1.15																		
1.20	16.84	5.75	64.8	15.40	6.02	61.2	15.40	6.37	58.9	16.68	5.83	64.4						
1.25																		
1.30	19.59	6.66	65.9	17.96	7.08	62.2	17.89	7.50	59.8	19.44	6.77	65.4						
1.35																		
1.40	22.54	7.62	66.8	20.69	8.21	63.4	20.50	8.65	60.6	22.29	7.80	66.1						
1.45																		
1.50	25.60	8.61	67.4	23.59	9.35	64.3	23.37	9.83	61.6	25.30	8.84	67.3						
1.55																		
1.60	28.85	9.63	68.6	26.66	10.55	65.3	26.34	11.12	62.3	28.56	9.92	68.2						
1.65																		
1.70	32.75	10.65	69.5	29.90	11.71	66.2	29.45	12.44	63.0	31.97	10.98	69.3						
1.75																		
1.80	35.75	11.70	70.4	33.28	12.95	66.8	32.72	13.78	63.8	35.47	12.11	70.1						
1.85																		
1.90	39.46	12.73	71.0	36.79	14.20	67.6	36.10	15.16	64.6	39.19	13.22	70.8						
1.95																		
2.00	43.28	13.79	72.0	40.39	15.47	68.0	39.59	16.51	65.4	43.03	14.27	71.8						
2.05																		
2.10	47.21	14.87	72.4	44.19	16.70	68.7	43.19	17.89	66.3	46.95	15.37	72.5						
2.15																		
2.20	51.22	15.97	72.9	48.06	17.98	69.0	46.97	19.27	67.3	51.00	16.39	73.3						
2.25																		
2.30	55.41	17.03	73.3	52.01	19.31	69.3	50.82	20.63	68.1	55.16	17.44	73.7						
2.35																		
2.40	59.66	18.20	74.1	56.03	20.62	69.6	54.78	22.00	68.4	59.41	18.41	74.2						
2.45																		
2.50	64.02	19.27	74.4	60.15	21.92	70.2	58.78	23.35	69.0	63.69	19.48	74.7						
2.55																		
2.60	68.42	20.34	75.3	64.39	23.26	70.8	62.93	24.69	69.6	68.08	20.51	75.2						
2.65																		
2.70	73.01	21.45	75.9	68.64	24.60	71.2	67.12	25.97	70.3	72.62	21.51	75.6						
2.75																		
2.80	77.52	22.49	76.5				71.33	27.29	70.6	77.13	22.54	76.2						
2.85																		
2.90	82.24	23.57	76.5				75.60	28.56	71.0									

TABLE 4 - TIME-POSITION DATA FOR PHASE 1b - CURVED VERTICAL TRAJECTORIES

Time	F-19			F-25			F-26			F-37			F-38		
Secs.	Depth in.	Long in.	Incl. deg.	Depth in.	Long in.	Incl. deg.	Depth in.	Long in.	Incl. deg.	Depth in.	Long in.	Incl. deg.	Depth in.	Long in.	Incl. deg.
	d_o=8.51	L_o=0.80	Θ_o=68.4	d_o=+0.06	L_o=-0.09	Θ_o=66.5	d_o=-0.36	L_o=-0.06	Θ_o=67.4	d_o=-0.20	L_o=-0.02	Θ_o=50.5	d_o=0	L_o=0	Θ_o=50.1
t_o	-0.29			+0.06			-0.06			-0.18			-0.04		
0	0	0		0	0	66.5	0	0	67.4	0	0	51.1	0	0	50.2
0.02	1.06	0.14	77.5	0.05	-0.06	66.5	0.24	-0 08	67.7	0.11	0.04	51.2	0.02	0	50.3
0.04	2.20	0.24	78.4	0.07	-0.02	66.5	0.56	-0.06	67.8	0.17	0.08	51.4	0.09	0	50.4
0.06	3.43	0.40	79.0	0.04	-0.04	66.5	0.97	-0.06	68.1	0.23	0.09	51.7	0.07	0	50.3
0.08	4.70	0.56	79.7	0.09	-0.08	66.7	1.44	-0.06	68.6	0.35	0.10	52.2	0.15	0	50.3
.10	6.04	0.72	80.2	0.18	-0.14	66.9	1.96	-0.08	69.1	0.46	0.16	52.4	0.16	0.01	50.5
.12	7.42	0.94	80.9	0.25	-0.22	66.9	2.57	-0.08	69.4	0.57	0.19	52.7	0.17	0.03	50.6
.14	8.90	1.10	81.4	0.46	-0.26	66.9	3.23	0.02	70.0	0.70	0.19	53.0	0.26	0.05	50.8
.16	10.42	1.26	81.8	0.69	-0.26	67.0	3.92	0.04	70.7	0.88	0.21	53.4	0.29	0.06	50.8
.18	11.93	1.50	82.2	1.02	-0.30	67.5	4.70	0.16	71.3	1.00	0.25	53.6	0.38	0.07	50.9
.20	13.51	1.68	82.6	1.39	-0.30	67.5	5.56	0.22	71.9	1.22	0.32	54.2	0.48	0.08	51.1
.22	15.23	1.84	83.0	1.85	-0.28	67.8	6.48	0.34	72.6				0.57	0.09	51.3
.24	16.97	2.04	83.3	2.36	-0.24	68.1	7.50	0.44	73.2				0.65	0.14	51.7
.26	18.75	2.22	83.6	2.95	-0.20	68.5	8.52	0.62	74.0				0.75	0.19	51.9
.28	20.56	2.44	84.0	3.58	-0.18	68.9	9.64	0.80	74.7				0.89	0.22	52.2
.30	22.45	2.62	84.2	4.34	-0.06	69.2	10.81	0.96	75.3	2.20	0.52	56.6	1.02	0.26	52.4
.32	24.37	2.84	84.6	5.10	0	69.9	12.08	1.10	76.1				1.14	0.28	52.7
.34	26.36	3.02	84.7	5.93	0.08	70.3	13.40	1.30	76.6				1.33	0.32	52.8
.36	28.36	3.24	85.0	6.84	0.22	70.8	14.78	1.46	77.1				1.48	0.37	53.2
.38	30.44	3.46	85.2	7.80	0.40	71.5	16.16	1.72	77.8				1.60	0.42	53.6
.40	32.60	3.64	85.3	8.84	0.54	72.2	17.63	1.90	78.3	3.37	0.80	58.8	1.80	0.46	53.9
.42	34.73	3.84	85.5	9.92	0.70	72.9	19.19	2.10	78.9						
.44	36.88	4.00	85.7	11.06	0.88	73.3	20.77	2.32	79.4						
.46	39.14	4.20	86.0	12.28	1.10	74.1	22.37	2.54	79.5						
.48	41.43	4.46	86.2	13.58	1.30	74.6	24.08	2.80	80.1						
.50	43.72	4.68	86.3	14.83	1.38	75.1	25.88	3.04	80.5	4.83	1.18	61.3	2.89	0.76	55.7
.52	46.03	4.84	86.5	16.17	1.62	76.0	27.67	3.26	80.5						
.54	48.45	5.08	86.7	17.63	1.88	76.2	29.47	3.50	81.1						
.56	50.90	5.28	86.7	19.13	2.10	76.9	31.38	3.68	81.5						
.58	53.32	5.50	86.7	20.73	2.38	77.3	33.35	3.92	81.9						
.60	55.81	5.68	86.8	22.35	2.60	77.7	35.36	4.14	82.3	6.54	1.59	63.8	4.09	1.12	57.9
.62	58.36	5.88	86.8	24.00	2.90	78.0	37.40	4.34	82.5						
.64	60.91	6.12	86.9	25.74	3.14	78.4	39.50	4.58	82.7						
.66	63.54	6.32	87.1	27.51	3.40	79.0	41.64	4.82	82.8						
.68	66.14	6.48	87.5	29.33	3.70	79.2	43.81	5.02	83.0						
.70	68.76	6.68	87.6	31.20	3.94	79.6	45.98	5.24	83.2	8.49	2.09	65.7	5.68	1.54	60.0
.72				33.13	4.22	79.9	48.26	5.48	83.6						
.74				35.11	4.50	80.2	50.57	5.70	83.9						
.76				37.15	4.78	80.6	52.86	5.94	83.9						
.78				39.21			55.20	6.14	84.0						
.80				41.27	5.36	81.0	57.56	6.36	84.2	10.64	2.64	67.8	7.47	2.07	61.9
.82				43.46			60.00	6.58	84.3						
.84				45.64	5.88	81.3	62.48	6.80	84.4						
.86				47.85	6.18	81.6	64.98	6.98	84.7						
.88				50.13	6.48	81.9	67.50	7.20	84.7						
.90				52.45	6.76	82.1	70.05	7.38	84.8	13.01	3.23	69.3	9.41	2.64	63.9
.92				54.77	6.98	82.2	72.69	7.62	84.9						
.94				57.19	7.28	82.3	75.30	7.84	84.9						
.96				59.58	7.54	82.4	77.88	8.00	84.9						
.98				62.01	7.84	82.5	80.58	8.18	84.9						
1.00				64.51	8.10	82.7	83.27	8.46	84.9	15.58	3.87	70.5	11.61	3.32	65.4
1.05				66.97	8.42	82.7									
1.10				69.51	8.70	83.0				18.39	4.50	72.1	14.01	4.02	67.0
1.15				72.05	8.96	83.2									
1.20				74.68	9.22	83.5				21.33	5.16	73.2	16.61	4.72	68.4
1.25				77.28	9.50	83.7									
1.30				79.93	9.76	83.7				24.51	5.81	74.2	19.37	5.55	69.2
1.35				82.61	10.08	83.7									
1.40										27.84	6.49	75.3	22.35	6.37	70.1
1.45															
1.50										31.38	7.16	76.2	25.50	7.23	71.1
1.55															
1.60										35.05	7.83	77.4	28.83	8.12	71.9
1.65															
1.70										38.87	8.47	78.2	32.32	8.97	73.0
1.75															
1.80										42.84	9.07	79.1	35.92	9.84	73.9
1.85															
1.90										46.92	9.67	79.8	39.71	10.73	75.0
1.95															
2.00										51.20	10.22	80.1	43.63	11.60	75.5
2.05															
2.10										55.47	10.78	80.5	47.67	12.47	76.2
2.15															
2.20										59.89	11.36	80.9	51.77	13.35	76.8
2.25															
2.30										64.47	11.92	81.2	56.02	14.15	77.5
2.35															
2.40										69.04	12.49	81.4	60.38	14.93	78.2
2.45															
2.50										73.67	13.05	81.8	64.82	15.74	78.8
2.55															
2.60													69.36	16.47	79.4
2.65															
2.70															

TABLE: B-1

COMPUTATION FORMULAS
FOR EXPANDING DATA TO FULL SCALE

DIMENSION	DESCRIPTION	EXPANSION FORMULA
L	HORIZONTAL DISTANCE — FT.	$= \lambda\,(2/12)\,\Sigma\,\Delta L$
D	VERTICAL DISTANCE — FT.	$= \lambda\,(2/12)\,\Sigma\Delta D$
Z	LATERAL DISTANCE — FT.	$= \lambda\,(2/12)\,\Sigma\,K\,\Delta Z$
S	DISTANCE ALONG TRAJECTORY — FT.	$= \lambda(2/12)\sqrt{\Delta L)^2+(\Delta D)^2 + (K\Delta Z)^2}$
t	TIME — SEC.	$= (\lambda)^{1/2}\,\Sigma\,(N/F)$
θ	INCLINATION ANGLE — DEG.	$= \theta_M = \theta_T$
ψ	AZIMUTH ANGLE — DEG.	$= \psi$ = arc tan $(K \tan \psi_T)$
ϕ	ROLL ANGLE — DEG.	$= \phi_M = \phi_T$
γ	TRAJECTORY ANGLE IN VERTICAL PLANE — DEG.	= arc tan $(\Delta V / \Delta L)$
η	TRAJECTORY ANGLE IN HORIZONTAL PLANE — DEG.	= arc tan$(K\Delta Z / \Delta S)$
α	ANGLE OF ATTACK IN VERTICAL PLANE — DEG.	$= \theta - \beta$
β	ANGLE OF ATTACK IN HORIZONTAL PLANE — DEG.	$= \psi - \eta$
V	VELOCITY — FPS.	$= (\lambda)^{1/2}\,(2/12)\,(F\Delta S/N)$
$\dot{\theta}, \dot{\psi}, \dot{\phi}$	ANGULAR VELOCITIES — RAD/SEC OR RAD/FT.	$= (1/\lambda)\,(12/2)\,(\pi/180)(\Delta\theta/\Delta S, \Delta\psi/\Delta S, \Delta\phi/\Delta S)$
$\dot{D}, \dot{Z}, \dot{L}$	RATE OF CHANGE OF DEPTH AND LATERAL — FT/FT	$= \Delta D/\Delta S, K\Delta Z/\Delta S, \Delta L/\Delta S$

TABLE B-2 LIST OF SYMBOLS AND SIGN CONVENTION

SYMBOL	DEFINITION	POSITIVE DIRECTION
L	HORIZONTAL DISTANCE	ALONG AXIS PARALLEL TO TANK CENTERLINE
D	DEPTH OR CHANGE OF DEPTH	DOWN FROM WATER SURFACE
Z	LATERAL	FROM TANK CENTERLINE TO BACK WALL
S	DISTANCE ALONG TRAJECTORY	ALONG DIRECTION OF FORWARD MOTION
t	TIME	FROM FIRST FRAME ANALYZED
θ	INCLINATION OF MODEL AXIS WITH RESPECT TO HORIZONTAL	FOR NOSE DOWN
ψ	AZIMUTH ANGLE OF MODEL AXIS WITH RESPECT TO VERTICAL PLANE CONTAINING TANK CENTERLINE	FOR NOSE TO STARBOARD
ϕ	ROLL ANGLE OF MODEL VERTICAL PLANE OF SYMMETRY	FOR HEEL TO STARBOARD
α	ANGLE OF ATTACK IN MODEL VERTICAL PLANE (INCLINATION)	FOR NOSE DOWN WITH RESPECT TO TANGENT TO TRAJECTORY
β	ANGLE OF ATTACK IN YAW IN PLANE OF TANGENT TO TRAJECTORY	FOR NOSE TO STARBOARD WITH RESPECT TO TANGENT TO TRAJECTORY
γ	ANGLE OF TANGENT TO TRAJECTORY WITH RESPECT TO HORIZONTAL	FOR INCREASING DEPTH
η	ANGLE OF TANGENT TO TRAJECTORY WITH RESPECT TO TANK CENTERLINE	FOR INCREASING LATERAL
δ_S	CONTROL SURFACE	FOR CAUSING MODEL TO TURN IN DIRECTION OF POSITIVE ANGLE
V	VELOCITY OF C.G. OF MODEL ALONG TRAJECTORY	—
λ	LINEAR SCALE FACTOR OF MODEL TO PROTOTYPE SIZE	—
F	FLASH RATE OF TANK HIGH SPEED LAMPS OR PICTURE FRAME RATE	—
N	NUMBER OF FRAMES ON FILM RECORD BETWEEN DATA POINTS OR FRAMES ANALYZED	—
K	CORRECTION FACTOR FOR LATERAL DIMENSIONS IN ANALYZER	—

TABLE B-3

READING AND POSITIONING ACCURACY IN TRAJECTORY ANALYZER

DIMENSION	STEREO - PROJECTION		SINGLE PROJECTOR
	VERTICAL PLANE	HORIZONTAL PLANE	
LONGITUDINAL - IN.	± 0.01	± 0.02	± 0.02
VERTICAL - IN.	± 0.01	± 0.01	± 0.02
LATERAL - IN.	± 0.02	± 0.03	± 0.05
INCLINATION - DEG.	± 0.1	± 0.1	± 0.2
AZIMUTH - DEG.	± 0.2	± 0.3	± 0.5
ROLL - DEG.	± 0.2	± 0.5	± 1.0

NOTE: LINEAR DIMENSIONS ARE ONE-HALF MODEL SIZE.

DISTRIBUTION LIST

Department of the Navy
Bureau of Ordnance
Contract NOrd-16200

Copy No.	
1-4	Chief, Bureau of Ordnance, Navy Dept., Washington 25, D. C. Attn: Code ReO-3
5-8	Chief, Bureau of Ordnance, Navy Dept., Washington 25, D. C. Attn: Code ReU
9-10	Chief, Bureau of Ordnance, Navy Dept., Washington 25, D. C. Attn: Code Ad3
11-13	Chief, Bureau of Aeronautics, Navy Dept., Washington 25, D. C.
14-18	Chief, Bureau of Ships, Navy Dept., Washington 25, D. C.
19-21	Chief, Office of Naval Research, Navy Dept., Washington 25, D. C. Attn: Code 438
22	Commanding Officer, Office of Naval Research Branch Office, 1030 East Green Street, Pasadena 1, California
23-24	Commanding Officer and Director, David Taylor Model Basin, Washington 7, D. C.
25-26	Commanding Officer, U. S. Naval Underwater Ordnance Station, Newport, Rhode Island
27-28	Commander, U. S. Naval Ordnance Laboratory, White Oak, Silver Spring, Maryland
29-30	Commander, U. S. Naval Ordnance Test Station, Pasadena, California
31	Commander, U. S. Naval Ordnance Test Station, China Lake, California
32	Director, Experimental Towing Tank, Stevens Institute of Technology, via: Bureau of Aeronautics Representative, c/o Bendix Aviation Corp., Eclipse-Pioneer Division, Teterboro, New Jersey
33	Director, Ordnance Research Laboratory, Pennsylvania State University, University Park, Pennsylvania
34	Alden Hydraulic Laboratory, Worcester Polytechnic Institute, Worcester, Mass., via: Inspector of Naval Material, 495 Summer Street, Boston 10, Mass.
35-36	Librarian, U. S. Naval Postgraduate School, Monterey, Calif.

DISTRIBUTION LIST

Department of the Navy
Bureau of Ordnance
Contract NOrd-18200

Copy No.	
1-4	Chief, Bureau of Ordnance, Navy Dept., Washington 25, D. C. Attn: Code ReO-3
5-8	Chief, Bureau of Ordnance, Navy Dept., Washington 25, D. C. Attn: Code ReU
9-10	Chief, Bureau of Ordnance, Navy Dept., Washington 25, D. C. Attn: Code Ad3
11-13	Chief, Bureau of Aeronautics, Navy Dept., Washington 25, D. C.
14-18	Chief, Bureau of Ships, Navy Dept., Washington 25, D. C.
19-21	Chief, Office of Naval Research, Navy Dept., Washington 25, D. C. Attn: Code 438
22	Commanding Officer, Office of Naval Research Branch Office, 1030 East Green Street, Pasadena 1, California
23-24	Commanding Officer and Director, David Taylor Model Basin, Washington 7, D. C.
25-26	Commanding Officer, U. S. Naval Underwater Ordnance Station, Newport, Rhode Island
27-28	Commander, U. S. Naval Ordnance Laboratory, White Oak, Silver Spring, Maryland
29-30	Commander, U. S. Naval Ordnance Test Station, China Lake, California
31	Commander, U. S. Naval Ordnance Test Station, China Lake, California
32	Director, Experimental Towing Tank, Stevens Institute of Technology, Hoboken, New Jersey; via: Bureau of Aeronautics Representative, c/o Bendix Aviation Corp., Eclipse-Pioneer Division, Teterboro, New Jersey
33	Director, Ordnance Research Laboratory, Pennsylvania State University, University Park, Pennsylvania
34	Alden Hydraulic Laboratory, Worcester Polytechnic Institute, Worcester, Mass., via: Inspector of Naval Material, 495 Summer Street, Boston 10, Mass.
35-36	Librarian, U. S. Naval Postgraduate School, Monterey, California

Contract NOrd-16200

DISTRIBUTION LIST (Cont'd)

Copy No.	
37-46	British Joint Services Mission, Navy Staff, via: Chief, Bureau of Ordnance, Navy Dept., Washington 25, D. C. Attn: Code Ad8
47-49	Commander, U. S. Naval Proving Ground, Dahlgren, Virginia
50-51	National Advisory Committee for Aeronautics, Langley Memorial Aeronautical Laboratory, Langley Field, Virginia
52	National Advisory Committee for Aeronautics, Lewis Flight Propulsion Lab., Cleveland Airport, Cleveland, Ohio
53	Director, National Advisory Committee for Aeronautics, 1512 H Street, N. W., Washington 25, D. C.
54	Director, National Advisory Committee for Aeronautics, Ames Laboratory, Moffett Field, California
55-56	Commander, Air Research and Development Command, Post Office Box 1395, Baltimore 3, Maryland
57	ASTIA Reference Center, Technical Information Division, Library of Congress, Washington 25, D. C.
58-63	Director, Armed Services Technical Information Agency, Documents Service Center, Knott Building, Dayton 2, Ohio Attn: DSC-SA

Copy No.

37-46 British Joint Services Mission, Navy Staff, via: Chief, Bureau of Ordnance, Navy Dept., Washington 25, D. C.
Attn: Code Adp

47-49 Commander, U. S. Naval Proving Ground, Dahlgren, Virginia

50-51 National Advisory Committee for Aeronautics, Langley Memorial Aeronautical Laboratory, Langley Field, Virginia

52 National Advisory Committee for Aeronautics, Lewis Flight Propulsion Lab., Cleveland Airport, Cleveland, Ohio

53 Director, National Advisory Committee for Aeronautics, 1512 H Street, N. W., Washington 25, D. C.

54 Director, National Advisory Committee for Aeronautics, Ames Laboratory, Moffett Field, California

55-56 Commanding Officer, Air Research and Development Command, P. O. Box 1395, Baltimore 3, Maryland

57 ASTIA Reference Center, Technical Information Division, Library of Congress, Washington 25, D. C.

58-61 Director, Armed Services Technical Information Agency, Documents Service Center, Knott Building, Dayton 2, Ohio
Attn: DSC-SA

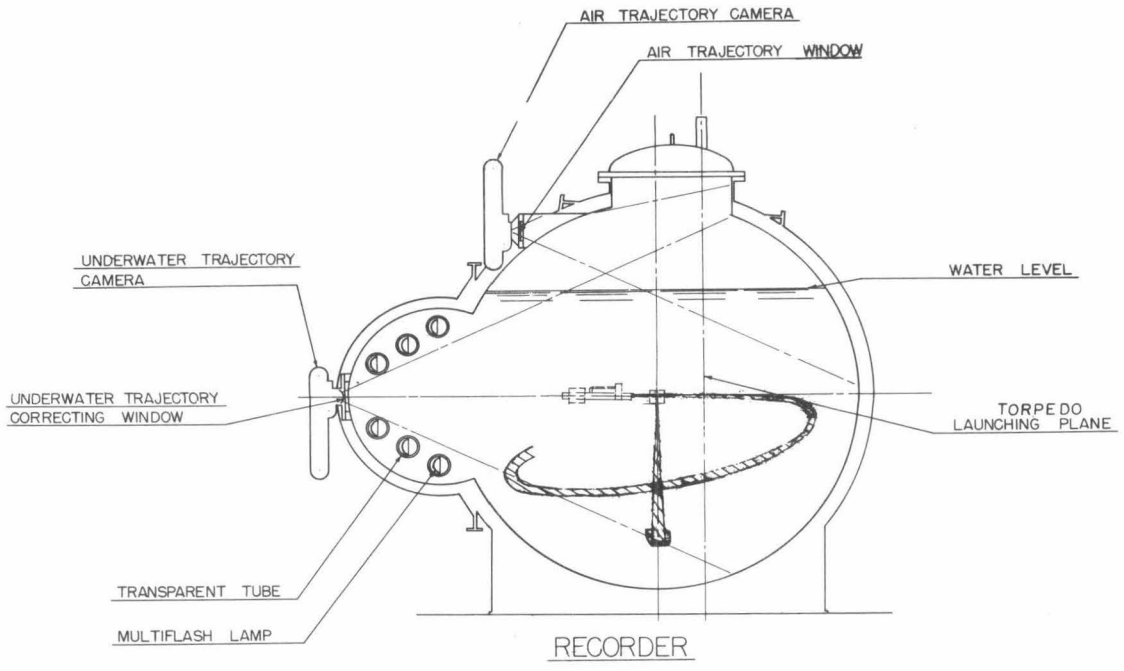

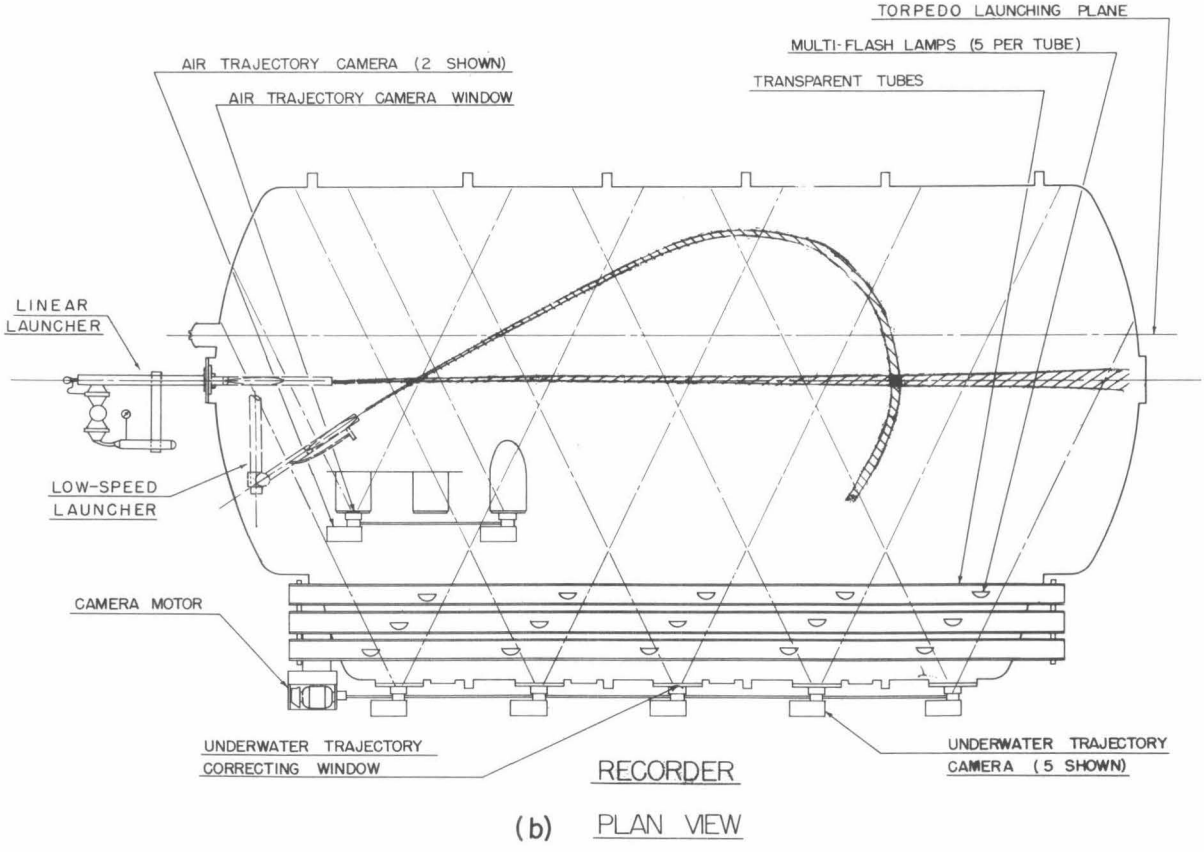

Fig. B-3 - Trajectory recording system: (a) end elevation, (b) plan view.

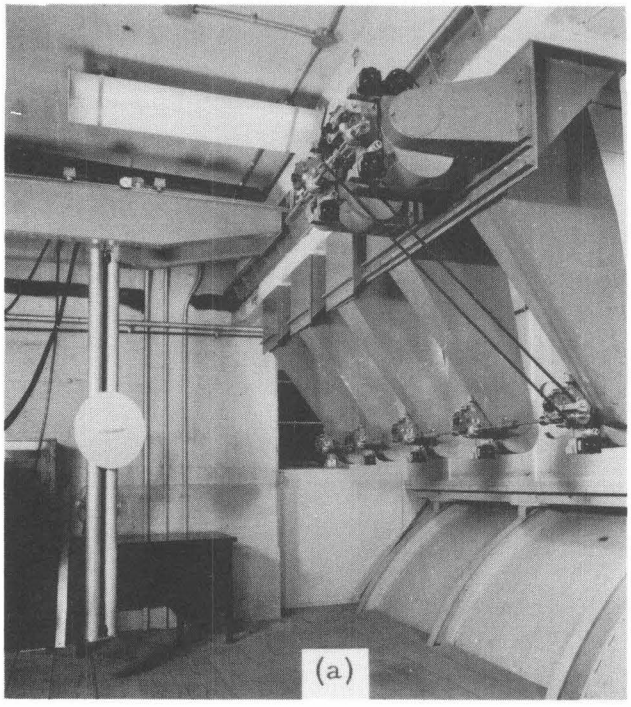

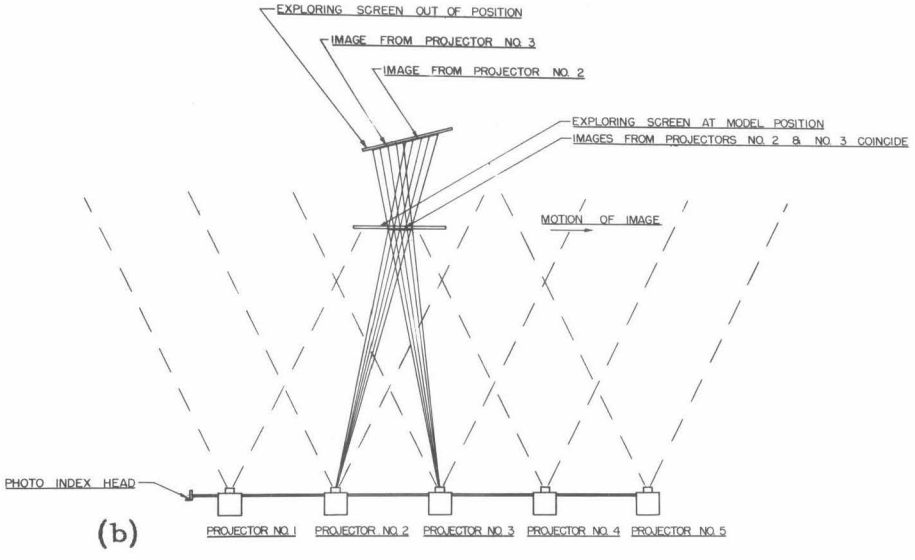

Fig. B-4 - Trajectory analyzing system: (a) view of analyzer room, (b) image aligning technique.